ELECTRIC FIELD OPTIMIZATION IN SF6 CIRCUIT BREAKERS

BY

SALEH. K. ABU HANIEH

A Thesis Presented to the

DEANSHIP OF GRADUATE STUDIES

KING FAHD UNIVERSITY OF PETROLEUM & MINERALS

DHAHRAN, SAUDI ARABIA

In Partial Fulfillment of the
Requirements for the Degree of

MASTER OF SCIENCE

In

ELECTRICAL ENGINEERING

MAY, 2012

KING FAHD UNIVERSITY OF PETROLEUM & MINERALS

DHAHRAN 31261, SAUDI ARABIA

DEANSHIP OF GRADUATE STUDIES

This thesis, is written by **SALEH KHAIRI SALEH ABU HANIEH,** under the direction of his thesis advisor and approved by his thesis committee, has been presented to and accepted by the Dean of Graduate Studies, in partial fulfillment of the requirements for the degree of **MASTER OF SCIENCE IN ELECTRICAL ENGINEERING.**

Thesis Committee:

Dr. ZAKARIYA AL-HAMOUZ (Chairman)

Dr. IBRAHIM EL-AMIN (Member)

Dr. MOHAMMED ABIDO (Member)

Dr. ALI AL-SHAIKHI
(Department Chairman)

Dr. SALAM ZUMMO
(Dean of Graduate Studies)

Date 1/8/12

In the name of Allah, the Most Gracious and the Most Merciful

Dedicated

to

My Beloved Parents and Brothers

ACKNOWLEDGMENTS

All praise and thanks are due to Almighty Allah, Most Gracious and Most Merciful, for his immense beneficence and blessings. He bestowed upon me health, knowledge and patience to complete this work. May peace and blessings be upon prophet Muhammad (PBUH), his family and his companions.

Thereafter, acknowledgement is due to KFUPM for the support extended towards my research through its remarkable facilities and for granting me the opportunity to pursue graduate studies as a part time student.

I acknowledge, with deep gratitude and appreciation, the inspiration, encouragement, valuable time and continuous guidance given to me by my thesis advisor, Dr. Zakariya M. AL-Hamouz. I am also grateful to my Committee members, Dr. Ibrahim EL-Amin and Dr. Mohamad Abido for their constructive guidance and support.

My heartfelt thanks are due to my parents and brothers for their prayers, guidance, and moral support throughout my academic life.

I extend a special thanks to Mr. Samer Mokdad for his support and guidance in my carrier's life.

Finally, special thanks are due to all professors and friends who made my study's life beautiful and easy.

TABLE OF CONTENTS

LIST OF TABLES

LIST OF FIGURES

THESIS ABSTRACT (ENGLISH)

NAME: **SALEH ABU HANIEH**

TITLE: **ELECTRIC FIELD OPTIMIZATION IN SF6 CIRCUIT BREAKERS**

MAJOR FIELD: **ELECTRICAL ENGINEERING**

DATE OF DEGREE: **MAY / 2012**

The objective of this thesis is to enhance the insulation capability (Increasing the breakdown voltage) in SF6 CBs by reducing the electric field concentration inside the insulation medium. To achieve that, the electric field Problem in the SF6 CB is formulated as an optimization problem. Two artificial intelligence techniques namely: particle swarm (PS) and simulated annealing (SA) where used to solve the objective function. A combined ANSYS-Artificial intelligence algorithms have been proposed.

The effectiveness of the newly proposed electric field optimization algorithms has been tested successfully on two SF6 CB's (252 kV and 550 kV) reported in the literature. The performance of the proposed methods outperformed the optimization results reported before.

Not only the electric field is highly reduced using the proposed algorithms but also the computational time is reduced too. Furthermore the effect of space charge on the performance of the proposed algorithms has been studied.

MASTER OF SCIENCE DEGREE

KING FAHD UNIVERSITY OF PETROLEUM AND MINERALS

Dhahran, Saudi Arabia

THESIS ABSTRACT (ARABIC)

ملخص الرسالة

الاسم: **صالح خيري أبو هنية**

عنوان الرسالة: **أمثلة المجال الكهربائي في القواطع الغازية**

التخصص: **الهندسة الكهربائية**

تاريخ التخرج: **جمادى الأخر /1433**

الهدف الرئيسي من هذه الأطروحة هو تحسين أداء العزل (رفع جهد انهيار العازلية) داخل القواطع الغازية عن طريق خفض قيم المجال الكهربائي داخل المادة العازلة. ولتحقيق ذلك, تم تمثيل المجال الكهربائي في قواطع الغاز التي تعتمد غاز سادس فلوريد الكبريت كمادة عزل على شكل مسألة ايجاد الحل الأمثل باستخدام طريقتين تعتمدان استخدام الذكاء الاصطناعي (PS) و (SA). تمت برمجة هذه الخوارزميات باستخدام لغة (APDL) الذي يعتمده برنامج (ANSYS) كلغة أوامر لأول مرة, حيث لم يسبق استخدام هذا الاسلوب من قبل في اي ورقة عمل.

ولاثبات كفاءة الطرق المقترحة في هذه الأطروحة, تم ايجاد الحلول المثلى لمسألة ايجاد المجال الكهربائي الأقل لقاطعي جهد عالي مذكورين في ورقتي عمل سابقتين ومقارنة النتائج مع ما تم ايجاده في تلكم البحثيين.

النتائج من استخدام الطرق المذكورة أفضل بكثير مما كتب من ابحاث في نفس الموضوع.

باستخدام الطرق المقترحة في هذه الأطروحة تم خفض قيم المجال الكهربائي بشكل كبير وواضح, أيضا تم خفض الوقت اللازم للحصول على النتائج بشكل كبير.

بالاضافة الا ذلك تم اختبار النتائج باعتبار وجود شحنات حرة داخل حجرة اطفاء الشرارة في القاطع.

شهادة ماجستير علوم
جامعة الملك فهد للبترول والمعادن
الظهران ، المملكة العربية السعودية

NOMENCLATURE

Greek Symbols

ρ_v	Volume charge density
ρ_s	Surface charge density
ε	Medium permittivity

Subscripts

$2D$	Two Dimensions
$3D$	Three Dimensions
ANN	Artificial Neural Network
$APDL$	ANSYS Parameters Developing Language
PSA	Particle Swarm Algorithm
BDV	Breakdown Voltage
CAE	Computer Aided Engineering
CB	Circuit Breaker
CSM	Charge Simulation Method
EF	Electric Field
EM	Electro Magnetics
FDM	Finite Difference Method
FEM	Finite Element Method
GA	Genetic Algorithm
GCB	Gas Circuit Breaker

SA	Simulated Annealing
$SF6$	Sulfur Hexafluoride.
VI	Vacuum Interrupter
CFD	Computational fluid dynamics
ANSI	American National Standard Institute
IEC	International Electrotechnical Committee

Superscripts

V	Electric Voltage
E	Electric Field Strength

CHAPTER 1

INTRODUCTION

1.1 OVERVIEW

The development of high voltage circuit breaker is a key issue to the development of the electric power system. The use of advanced computer technology and scientific calculation for the high voltage SF6 circuit breaker has become one of the main contents in the research field. If the arc-quenching chamber structure is known, the accrual numerical calculation of the electric field is a forward problem, optimizing the chamber structure according to the electric field requirement is an inverse problem solution, and it is more important since the SF6 gas is very sensitive to the electric field uniformity. The breakdown voltage of SF6 gas in uniform electric field is three times as that for air, while in non-uniform electric field it is close to air. The electric field around the contacts and nozzle is more non-uniform in SF6 CB [1].

Calculation of electric fields with the aid of computers is now an inevitable tool in various electricity-concerned technologies, in particular, for analyzing discharge phenomenon and designing high voltage equipments.

1.2 THESIS MOTIVATION AND OBJECTIVES

The insulation breakdown is considered as one of the major problems which affect the performance of power system components/devices, and hence reduces the overall reliability of the power network. High voltage circuit breakers, like any other high voltage component (insulators, bushings, etc), are affected by insulation breakdown problem.

In general, the insulation medium capability (or breakdown voltage) for these components can be improved by reducing the electric field concentration especially at the sharp edges to avoid any possible breakdown.

In this thesis, the SF6 circuit breaker has been studied in order to increase the breakdown voltage inside the breaking chamber.

The objectives for this thesis can be summarized as follow:

- To enhance the insulation performance of a high voltage SF6 circuit breaker by reducing the maximum electric field through uniforming the field inside the insulation medium.
- As opposed to all methods reported in the literature, the electric field enhancement has been formulated as an optimization problem in which optimum parameters of the design variables have been made using two optimization algorithms; namely: Particle Swarm (PS) and Simulated Annealing (SA) were used along with ANSYS software.
- Testing the performance of the newly designed circuit breaker by comparing results with what has been reported in the literature.

1.3 THESIS APPROACH AND METHODOLOGY

This work can be divided to the following stages:

- Literature survey was carried out on the breakdown problem in HV equipments.
- Literature survey was carried out on the electric field based breakdown problem in HV equipments.
- Literature survey was carried out on the breakdown problem in HV circuit breakers because of electric field.
- Literature survey was carried out on the electric field optimization in HV equipments in general.
- Literature survey was carried out on the electric field optimization in HV circuit breakers.
- A brief literature survey was carried out on the evolution history of high voltage circuit breakers and the tests which CBs have to pass to be part of the power system.
- Formulation of electric field problem for CB's as an objective function to be minimized subject to constrains.
- The outcomes of literature survey on high voltage SF6 circuit breakers were reproduced (two different cases).
- The proposed approach was used to solve the same cases which were found in the literature and the results were compared.

1.4 THESIS CONTRIBUTIONS

The contributions of this thesis in the field of high voltage equipment design are illustrated as follow:

- The proposed approach presents a solution to enhance the insulation performance for many high voltage equipments such as: post insulators, bushings, gas insulated/air insulated switchgears and circuit breakers.
- The proposed approach presents fast convergence techniques to reduce the design cost for the high voltage equipments.
- The proposed problem formulation and proposed approach were tested for different cases reported in the literature.

1.5 THESIS ORGANIZATION

The remaining chapters in this thesis are organized as follow:

Chapter 2 contains literature survey about breakdown in electrical equipments in general, electric field based breakdown in HV equipments, breakdown of HV circuit breakers due to electric field, optimization of electric field in electrical equipments, optimization of electric field in HV circuit breaker and brief literature survey about high voltage circuit breakers including the tests which are conducted. Chapter 3 addresses the optimization problem formulation and Finite Element Method principle (FEM) in solving partial differential equations. Chapter 4 presents the proposed algorithms to solve the optimization problem. Chapter 5 presents the simulation results for the two tested cases. Chapter 6 presents the conclusions and the recommendations for the future researchers.

CHAPTER 2

LITERATURE REVIEW

This chapter presents a literature survey about breakdown in electrical equipments in general, electric field based breakdown in HV equipments, breakdown of HV circuit breakers because of electric field, optimization of electric field in electrical equipments, optimization of electric field in HV circuit breaker and brief literature survey about high voltage circuit breakers including the tests which are conducted.

2.1 BREAKDOWN IN HIGH VOLTAGE EQUIPMENTS

According to [2], Electrical equipment has been known to fail by voltage stress (surface or internal discharges), by mechanical stress, by environmental conditions of heavy humidity, or chemical contaminants.

For safe and reliable operation of insulation systems, the dielectric properties of the insulation material, the manufacturing process and the insulation structure are most definitely addressed. Over the past decades, a series of changes have taken place in high voltage insulation systems [3].

Fofana et al [4] showed that moisture is enemy number one for transformer insulation, whereas in [5] & [6] the necessity of understanding the electric field and potential distribution in the transformer insulation system was highlighted, especially for the

designers to reduce the size and weight of electrical equipment in order to remain their companies' in the trade competition.

It is known that any metal particle contaminants present in the gas, produced for example from mechanical abrasions, can have a harmful effect by drastically lowering the corona onset and breakdown voltages. However, there is relatively little information available on how these effects depend on the particle shape, size, specific gravity and conductivity, the type of gas and gas pressure, the waveform of the applied voltage and the electrode configuration. It is essential that these effects be investigated in order to obtain design data for compressed-gas insulated high voltage equipment and to gain some insight into the pre-breakdown and breakdown processes. It has been observed that alternating voltage breakdown characteristics in compressed SF6 in the presence of free conducting particles are markedly dependent on particle shape, size, and material [7]. The presence of contaminating particles has long been recognized as a major limitation on the voltage insulating ability of compressed gases. Cases of failures in gas insulated substations and transmission lines have involved particles as a suspected cause and include breakdown with the gas gap alone and with dielectric surface flashover [8]. Filamentary conducting particles greatly reduce the ac breakdown voltage in compressed SF6, the effect becoming more pronounced with increasing particle length. The micro discharge and field enhancement mechanisms both appear to play important parts in particle-initiated gas breakdown. The relative contributions of each cannot be determined exactly, but the present results indicate that the effectiveness of either depends upon the particle motion and the experimental conditions [9]. Yet in contrast to liquids and solids, there are too few molecules to cause significant polarization effects and so electrical losses can be

vanishingly small. Because dielectric losses are extremely low, the common limitation for gaseous insulation is electrical breakdown [10].

The temperature and gas density distributions caused by the hot gas had taken into account in addition to the electrical field imposed across the gas by Uchii et al [11], the dielectric withstand of the hot gas can be much lower than that of unheated gas. Thus, the hot gas can lower the dielectric capability between the grounded tank and the high voltage interrupting chamber of the SF6 CB. Recently, gas CBs have been made increasingly compact, and the decrease in dielectric capability due to hot gas has become an important engineering problem in the development of GCB.

To develop a compact and reliable dead tank GCB, the behavior of hot gas flow and mechanisms of ground fault phenomena must be understood and accommodated during design stage. Despite a high electrical field strength outside the exhaust tube and lower field inside, the ground fault started inside the exhaust tube because the dielectric withstand of the hot gas within the tube is very low, which provides a weak-point for the initiation of breakdown.

The breakdown voltage (BDV) of SF6 gas under a uniform electrical field is a function of both density and temperature, for gas temperatures below 800K, the BDV under a uniform electrical field is proportional only to gas density, which is well known as paschen's law, above this temperature the BDV is lower value than predicted by paschen's law as a result of thermal dissociation or ionization of SF6 molecule [12].

Farahani et al in [13] have illustrated the insulation system of high voltage rotating machines, according to the aforementioned paper the insulating system is stressed during

operation by several factors like temperature, electrical field, and/or mechanical forces stresses the insulation is more strongly affected compared to purely additive application. Temperature and electrical field are of special importance for the aging procedures. In practice the electrical stress plays the main role in the development of insulation deterioration and the final breakdown, while other stresses such as thermal, mechanical, thermo-mechanical and environmental stresses are mostly the inception factor for creation of defects in insulating systems. The electrical stress can cause partial discharges in voids and cavities, which erode insulating materials and may lead to electrical treeing, which is often referred to as the most important degradation mechanism in solid insulations.

Another research [14] has been published to study the behavior of the insulation systems for high voltage rotating machines under different stresses, One of the most important insulation deterioration mechanisms in rotating machines is thermo-mechanical stresses during the machine's life caused by on-off operations or load changes. With these load changes, the insulation is thermo-mechanically stressed and ages because of the different thermal expansion coefficients of the materials involved and because of local and temporal gradients.

When the load on the machine is rapidly increased, the temperature of the copper rises quickly because of the I^2R losses, while the temperature of the insulation increases more slowly. Along the length of a long stator bar, a considerable shear stress between the copper and insulation will occur. If the insulating system cannot resist this shear stress, the bond between the copper and insulation may break and/or the laminated layers in the ground wall may tear or fatigue. Electrical stress which caused by the electric field

distribution can lead to insulation degradation because of (Partial Discharge) PD activity within the insulation adjacent to the conductor or in the bulk of the ground wall. The electrical stress can lead to electrical treeing, which is often referred to as the most important degradation mechanism in solid insulation.

We can conclude from [13] and [14] that the main two factors of breakdown in the rotating machines are the electric field and the thermo-mechanical factor.

Pfeiffer in [15] has studied the stresses on solid insulator. In practice, as far as electric stress is concerned, two failure mechanisms of solid insulation are relevant. Due to dielectric losses at high electrical stress, increased heating will occur, which may lead to thermal instability and thermal breakdown. This usually takes place within a few minutes and can be verified rather easily. The other major mechanism is the short-time breakdown field strength. Additionally, solid insulation systems typically also include gas gaps or voids either caused by different layers of insulation and interfaces or by improper manufacturing of the solid insulation material. In those small gaps partial discharges are very likely to occur at much lower field than being typical for the withstand capability of solid insulation.

Volat and Farzaneh [16] illustrated the effect of ice on the field distribution in solid insulators. They ended up that ice shedding during a melting period that modifies the number of air gaps (which affects the potential distribution along the ice-covered insulator) and the air-gap length (which affects the value of mean critical electric field) can considerably affect the development of flashovers along an ice-covered station post insulator.

In [17], another team of researchers worked on the charge profiles in XLPE cable under high electric fields. Space charge will have to be considered since its accumulation under a dc electric field is thought to be much more significant than that under ac fields. Space charge measurement in insulating materials had been done using conventional techniques such as the Thermally Stimulated Current (TSC) and the thermal pulse methods.

Cao et al [18] introduced a new trend in the dielectric industry by studying the nanodielectrics technology. According to their research, the fundamental understanding of dielectric properties at the nanoscale level is of great importance in the development of functional nanodielectrics for the electric power industry. More than ever such development needs will require close cooperation between industry and academia. Major original equipment manufacturers for example are already investing tremendous research and development effort and resources to position themselves for the coming challenging decade.

2.2 ELECTRIC FIELD BASED BREAKDOWN IN HIGH VOLTAGE EQUIPMENTS

In order to judge the breakdown behavior of high voltage arrangements it is important to know the field strength distribution especially the maximum value [19]. The knowledge of the field and the potential distributions at the dielectric insulation has always been important as a consequence of the general requirement to reduce the physical size of HV systems and to assure a high degree of reliability in operation. Improvement of HV systems reliability demands progress in the design criteria as well as a better understanding of the insulation behavior. The maximum values for the electric field along the dielectric/vacuum interface increase with higher dielectric permittivity materials [20]. Control of the electric field within and around high voltage equipment such as transmission line conductors, insulators and associated line hardware, surge arresters, switchgear, power transformers and rotating machines, is a very important aspect of the design of such equipment. Possible consequences of high levels of electric field are audible noise, radio noise, partial discharge and premature aging of insulation. Such effects can be evaluated strictly via laboratory experiment on full-size equipment or, in some cases, on “mock up” representations of the parts of the equipment of particular interest. Such testing can be very time consuming, often requiring a number of “trial and error” tests to determine dimensions and geometry which will result in satisfactory performance. The overall “design optimization” process can be greatly accelerated through the use of numeric electric field analysis. It is now possible to perform electric field analyzes of quite complex geometry on quite modest desk-top computers. However, for expediency and speed of computation, it is often desirable to simplify the geometry

[21]. In the aforementioned paper, electric field analysis programs based on a boundary element method have been employed to study the electric field and potential distribution along nonceramic insulators, and to demonstrate the influence of various aspects of line and tower geometry on the electric field along the insulators.

Many examples have been investigated during more comprehensive studies of practical problems encountered in recent years, demonstrate how the electric field and if necessary gradient distributions of certain high voltage equipment can be determined using the general-purpose program [22].

According to [23], the maximum dielectric strength for a gaseous insulator is obtained when electrode configurations produce uniform field distribution in the gap. However, in most of the practical applications, non-uniform field gaps are unavoidable.

The excellent insulation performance of SF6 is however only realized in uniform electric fields. If SF6 is used in non-uniform electric fields, its insulation performance is greatly reduced. To design compact GIS therefore, as uniform an electric field as possible must be achieved. It is well known that the insulation characteristics of SF6 under a uniform or quasi-uniform electric field greatly depend on local electric fields. When designing a GIS, electric field calculations are essential and GIS can be made optimal and economical only through the use of these calculations [24]. Most of the available publications, however, concentrate on the discharge characteristics of SF6 as a function of gap length and pressure. While a variety of electrode configurations was considered, the attention was not focused on the effect that a methodical variation of the radius of curvature of the electrodes may have on the breakdown characteristics. If the radius of curvature of a

given type of configuration is allowed to take a great number of values, interesting breakdown properties of the SF6 are observed which may be useful in the design of high voltage apparatus [25]. According to [7], the precise mechanisms causing breakdown in the compressed gases under contaminated conditions are not completely understood. One of the major mechanisms which might explain particle-initiated breakdown is the electric field at the particles. From the long history of troubleshooting, it is apparent that once a foreign metallic particle enters the insulation system, the breakdown voltage is significantly reduced and electric field calculation will be necessary to avoid the discharges from microstructure parts [26].

The main hazard in GIS comes from free metallic particles, which can move and cause breakdown under the influence of the electric field. Failure can also occur from highly stressed points accidentally left on a conductor, or from the repeated sparking of a floating electrode [27]. Sato et al [28] suggested a solution to solve this problem in GIS, they proved that composite insulation in the form of metallic electrodes coated with insulation is effective in reducing electric field strength and increasing breakdown voltage. It was clarified that there is an optimal thickness of insulation coatings which reduces electric field strength and the effects of reducing relative permittivity was shown. It was also shown that the field-reducing effect was prominent in a non-uniform electric field. Consequently, the study enabled the insulation distance in the gas gap to be reduced and made a great contribution towards reducing the size of the GIS.

In transformer, Qin et al [6] explained the necessity of computer program as an important tool for the transformer insulation design. It has been used to identify regions of high field strength where electrical breakdown might occur. Vogelsang et al [29] showed that

the electrical tree propagation (as a result of electric field stress) is the main electrical degradation mechanism leading to breakdown of high voltage winding insulation.

Capacitor is a simple electrical device compared to other electrical equipment, the electrical stresses within it are probably the highest of any common insulation system [2]. This is why a precise electric field distribution study should be conducted to ensure the safe use of a certain capacitor design. Another paper was proposed to study the breakdown in generator circuit breaker capacitor by Andjelic and Sadovic in [30].

In [31], high resistance surface coating of solid insulating components in highly stressed HVDC insulation systems have been investigated. The field distribution of HVDC insulation systems can be improved by using conductive surface coating. If a temperature increase due to power losses in the coating is avoided the resistance, is independent on the voltage and electric field stress.

2.3 BREAKDOWN IN HIGH VOLTAGE CIRCUIT BREAKERS DUE TO ELECTRIC FIELD

Manufacturers have focused on reducing the cost of interrupter components by adapting to more efficient contact geometry, improved contact materials, finite element modeling for improved field distribution and new processing techniques. Electric field analysis can be used to find the electric stress distribution to help the design of insulation that is adequate at the various applied voltages required under test and installation [32].

Due to the size reduction constraints of Gas Circuit Breaker (GCB), the hot gas during its dielectric recovery can be exposed (near the grounded tank or the exhaust tube) to high electrostatic fields leading to undesirable gas breakdown [33].

The transient breakdown voltages between the contacts could be calculated with high accuracy by combination of the gas flow analysis, electric field analysis and breakdown stress of SF6 gas. The transient breakdown voltages were generally lower than the static values obtained for stationary contacts and SF6 gas. This voltage decrease was closely connected with the transient pressure drop on the contacts. The transient breakdown voltage and pressure characteristics varied with nozzle shape. In an optimum nozzle the pressure drop was small and the transient breakdown voltages were high [34].

Nitta and Shibuya in [35] explained the effect of space charge in the breakdown voltage in SF6 breakers. At high pressure, the experimental discharge voltages reduce considerably from the theoretical values, and sometimes breakdown occurs under condition where even the maximum field in the gap is less than the value required. This

was explained as the effect of field distortion by negative space charge produced by field emission of electrons from the cathode.

For Vacuum Circuit Breakers (VCB) and Vacuum Interrupter (VI), Okubo in [36] showed that in recent years, optimization techniques of electric fields and electrical insulation, based on numerical analyses, such as CSM (Charge Simulation Method) have been introduced and have shown the significant effects on the development of the high voltage VI. It can be said that the electrode materials development, electrode conditioning and area effect of breakdown will be the critical techniques, especially under the non-uniform and long gap electrode configurations. In addition, the surface charging mechanism should be clarified to avoid the creepage discharge inception, under the higher average field VI. Computer aided optimization techniques for electrical insulation performance are considered to be introduced in the future.

In [37], the 84 kV class vacuum gap breakdown and surface flashover are summarized by the area effect. The multi-gap configuration remarkably increases the flashover voltage. The investigation results have contributed to size reduction of the vacuum interrupter/vacuum circuit breaker. Finally cubicle type GIS (C-GIS) housed the vacuum interrupter/vacuum circuit breaker was reduced as well.

Schumann et al [38] studied the breakdown voltage of electrode arrangements in vacuum circuit breakers. They reported that in the main contacts the HV strength decreases with growing electrode diameter. The measurement indicates a strong influence of the surface roughness on the HV strength. Smoother surface conditions lead to a higher dielectric strength, as would be expected. In order to increase the HV strength of shield electrodes

it is more effective to increase the gap between the electrodes than to enlarging the electrode radius.

Statistical property of the breakdown in vacuum was experimentally studied in [39]. The results was used to have an expression for cumulative breakdown probability of the contact of a vacuum circuit breaker as a function of applied voltage (V) and contact spacing (d).

2.4 ELECTRIC FIELD OPTIMIZATION IN HV EQUIPMENTS

Electric field optimization has been used in large scale recently to enhance the design of many electrical components.

Electric field computation to optimize the design of gas filled high voltage composite bushings was published by Monga et al in [40]. The United States Navy employs these bushings in high power very low frequency/low frequency transmitting stations. Commercially available 2D and 3D computational packages based on the boundary element method were employed to analyze the electric fields. The optimized design uses both internal and external elements for electric stress grading at critical parts of the bushing. It has been shown that the location and magnitude of the maximum electric field have been optimized which should result in a substantially higher corona free operating voltage. It has been demonstrated that the use of the 2-D model can be used effectively for optimizing the design of HV bushings. The optimum design consists of one corona ring at the top and an internal metal electric field shaper. Adding additional internal or external corona rings did not significantly change the magnitude or the location of the maximum electric field when compared to the optimized design.

The design of high voltage systems and their components (e.g. gas insulated switchgear, transformers etc.) is governed by the goal of reaching maximum reliability with a minimal need of material and space. A substantial prerequisite in order to reach this goal is an optimal electric field strength distribution on electrode, surfaces and dielectric boundaries. Such an optimal field strength distribution can he found using appropriate numerical optimization algorithms in combination with numerical field calculation

methods. A mathematical optimization algorithm is an algorithm that tries to find an optimal set of parameters for which a given objective function reaches a minimum. In order to utilize such an algorithm for high voltage engineering problems it is necessary to generate the geometry to be optimized depending on the parameters delivered by the optimization algorithm. Furthermore, it is desirable to optimize complex three dimensional field problems within a minimum computation time [41].

A new method for optimization of high voltage electrode contours based on Genetic Algorithms (GA) techniques has been presented in [42]. The method seeks the optimization of the electrode shape in order to achieve a uniform field distribution along the electrode surface while maintaining the maximum field stress at a minimum value. A practical example of an axisymmetric single-phase GIS bus termination is considered.

2.5 ELECTRIC FIELD OPTIMIZATION IN HV CIRCUIT BREAKERS

Designing a circuit breaker is a very complicated task since a lot of parameters have to be considered to pass the type test which will be illustrated next section.

The major two parameters can be summarized as follows:

- The circuit breaker should be able to carry the required current without permanent damage during all possible circumstances (normal and transient).
- The circuit breaker should be able to maintain the insulation level without breakdown inside the insulation medium during all possible conditions (normal and transient).

The fundamental equations to evaluate the voltage inside any medium are Poisson's equation and Laplace's equation.

The Poisson's equation in 3-D is given by:

$$\frac{\partial^2 V}{\partial x^2} + \frac{\partial^2 V}{\partial y^2} + \frac{\partial^2 V}{\partial z^2} = \frac{-\rho_v}{\varepsilon} \tag{2.1}$$

The Laplace's equation in 3-D is given by (by assuming that no space charge $\rho_v = 0$)

$$\frac{\partial^2 V}{\partial x^2} + \frac{\partial^2 V}{\partial y^2} + \frac{\partial^2 V}{\partial z^2} = 0 \tag{2.2}$$

The electric field can be evaluated by taking the gradient of the obtained voltage.

Perhaps the simplest among many partial differential equations that express physical phenomena among various numerical calculation methods, Finite Difference Method (FDM) and Finite Element Method (FEM) are very unique as they have been applied exclusively to electric field calculations. Fundamental difference between FDM and FEM is that, FDM can be used for calculation of potential at nodes only but FEM can be used for calculation of potential at nodes as well as within the elements. Furthermore, FEM much gives much accurate results for the geometries which have curvatures.

Calculation of electric field in 3D arrangement poses no essential problem by of the numerical methods if the field is given by Laplace's equation. The difficulty is that, it usually requires tedious work in preparing the input of a large amount of errorless data associate with 3D conditions.

Numerical solution of electromagnetic (EM) problems started in the mid of sixties with the availability of modern high-speed digital computers. Since then, considerable effort has been expended on solving practical, complex EM-related problems.

The finite element method has its origin in the field of structural analysis. The method was not applied to EM problems until 1968. Like the finite difference method, the finite element method is useful in solving differential equations. As finite difference method represents the solution region by array of grid points, its application becomes difficult with problems having irregularly shaped boundaries, such problems can be handled more easily by using the finite element method.

The finite element analysis of any problem involves basically four steps which are:

- Discretizing the solution region into a finite number of sub regions or elements.
- Deriving governing equations for a typical element (set of algebraic equations).
- Assembling all the elements in the solution region.
- Solving the system of equations obtained.

Few papers have been presented to solve this problem in CB. In [43], this problem was solved for 2D geometry of 550 kV SF6 breaker chamber, the authors reported that it was the first time for such complex structure of high voltage SF6 arc quenching chamber to be optimized. Using Variable Interval Genetic Algorithm (VIGA), the radius of curvature of the movable and stationary contacts are used as optimization variables, minimum of the ratio between maximum electric field and the average one is regarded as objective function in order to achieve more uniform distribution of the electric field, as a result the insulation capability of the arc quenching chamber for the same breaker was improved. The electric field in the optimized geometry was reduced by 37.2% from the initial geometry value, the electric field is calculated at six points (nodes) only, the reported optimization time is more than 8 hours (28975.891 s).

Hongxia et al [1] solved the same problem for 2D geometry of 252 kV SF6 breaker chamber since the 3D electric field in arc quenching chamber can be simplified to 2D due to the axisymmetric characteristic of the structure. Using zero-order method from the ANSYS optimization design tool, the shapes of nozzle and contacts are selected as optimization variables and the minimum of maximum electric field is regarded as optimization function.

A decent effort has been introduced by a group from Dalian university of technology in china [44]. The aim was to uniform the electric field distribution in the Vacuum Interrupters (VIs) especially in the high voltage range since it's not common to use the VIs interrupters in this voltage range. As it needs multi-breaks points in the same breaker, the authors used ANSYS software for electric field calculation and optimization where the distances between the shields are the optimization parameters.

In [45], another team of researchers worked on (VIs) where the optimized parameter was the floating potential electrode shape (the center shield of VI). Using Charge Simulation Method (CSM), the maximum electric field was reduced to 70% of none optimized shape.

According to the research of Yundong et al [46], the nozzle of SF6 CB is regarded as the main component of arc quenching chamber. This has been considered due to its controlling effect on dielectric recovery characteristics of the SF6 CB directly during the breaking process, the dielectric recovery in the course of interruption is an important qualification to judge the performance of the high voltage breaker. ANN and GA have been combined to achieve the optimal nozzle structure, the objective function of the nozzle optimization is to maximize the minimum dielectric recovery voltage in such way that it will withstand at least twice of the peak value of power frequency voltage , the optimized outcome was verified by Computer Aided Engineering (CAE) simulation, in this approach the dielectric recovery can be predicted accurately, the judgment condition was taken as the four parameter curve of the 252 kV SF6 CB to identify the performance. Comparing dielectric recovery with four parameter curve under different nozzle structures, if the dielectric recovery of CB is more than four parameter curve, this shows

that the CB has a good performance, finally the results were excellent and the dielectric recovery voltage raised by 7%.

In [47], a group of Korean researchers worked also in improving the dielectric recovery voltage for 170 kV GCB by minimizing the difference between the withstanding voltage and the applied one, using the evolution strategy as an optimization tool, the nozzle shape geometry was the design variable.

The optimized parameters in [11] are the inner diameter for the exhaust tube and the distance between the mouth of the exhaust tube and the tip of the arcing contact, this paper shows that as the length of the exhaust tube increases, the hot gas at the mouth cools, causing the critical BDV to rise, about optimization technique, the measured data and the result of the electric field analysis were compared, and as a result suitable parameters were chosen accordingly.

2.6 HIGH VOLTAGE CIRCUIT BREAKERS (HVCB)

High Voltage Circuit Breaker (HVCB) designed for operation of the electric network under normal conditions as well as for the interruption of faulted conditions, HVCBs have played an important role in power systems over 100 years [48].

The circuit breaker is a switching device which can open or close a circuit in a small fraction of second. This is achieved due to its separable contacts. The closing and opening of the circuit allows to establish or to interrupt the circulation of current through the circuit under usual or unusual working conditions, such as short circuits [48].

The major types of circuit breaker can be grouped based on the insulation medium and according to the invention history which is shown in Fig. 2.1 as follows:

- Air Blast Circuit Breaker (ABCB).
- Oil Circuit Breaker (OCB).
- SF6 Circuit breaker (GCB).
- Vacuum Circuit Breaker (VCB).

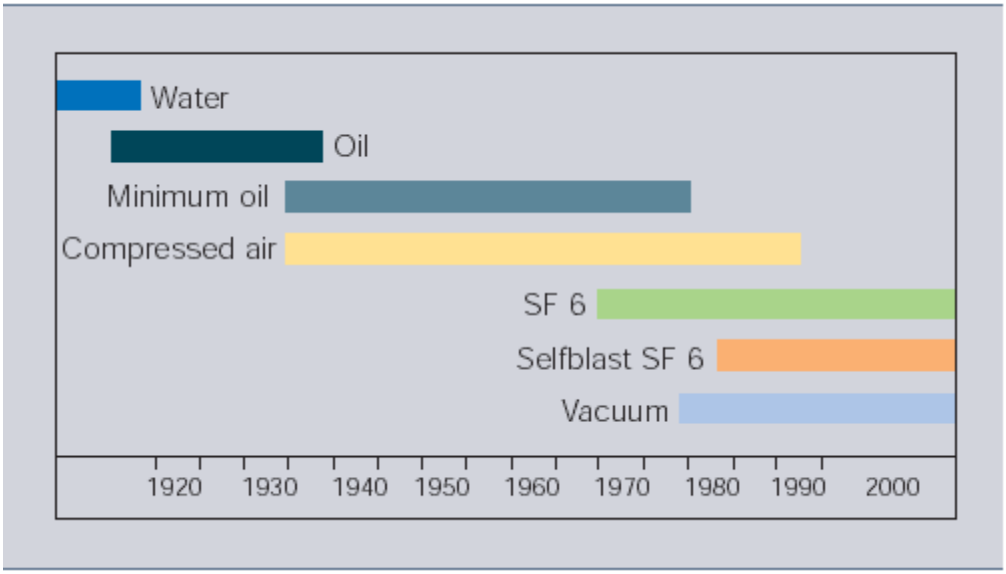

Figure 2.1 CB evolution history [49]

2.6.1 Air Blast Circuit Breaker (ABCB)

Air blast circuit breakers (also called compressed air circuit breaker) were used before 1980s for 11 to 1100 kV. A compressor plant is necessary to maintain high air pressure in the air receiver. 500 kV ABCB is shown in Fig. 2.2.

During the period 1950-1970, ABCB were preferred for 220 kV and above. However today, SF6 circuit breakers are preferred for this range. For 11 kV and 33 kV applications VCBs are preferred, ABCB have become obsolete in 1995 [50].

Figure 2.2 (500 kV) ABCB

2.6.2 Oil Circuit Breaker (OCB)

Oil circuit breaker can be classified based on the amount of oil used to the followings:

- Bulk Oil Circuit Breaker.
- Minimum Oil Circuit Breaker.

The bulk oil type was widely used for rated up to 72.5 kV before 1960. However the popularity of this breaker is decreasing and no more favored in modern installation [50], the contacts of the breaker are completely immersed in the oil. A 66 kV bulk oil circuit breaker is shown in Fig. 2.3.

Due to the necessity of large amount of oil and the big size of the tank this type of OCB were completely replaced by the minimum oil circuit breaker.

Figure 2.3 (66 kV) Bulk oil circuit breaker

The minimum oil type is also known as poor oil or small oil circuit breaker, in minimum oil circuit breaker the current interruption takes place inside ‘interrupter’, the enclosure of the interrupter is made of insulating material like porcelain. Hence the clearance between the live parts can be reduced and lesser quantity of oil require for internal insulation [50]. Fig. 2.4 shows a 66 kV minimum oil circuit breaker.

Figure 2.4 (66 kV) Minimum oil circuit breaker

Minimum oil circuit breakers have the following disadvantages:

- Short contact life.
- Frequent maintenance is required.
- Possibility of explosion.
- Larger arcing time for small currents.

They are being superseded by SF6 circuit breaker in all ranges [50].

2.6.3 SF6 Circuit Breaker (GCB)

Sulphur hexafluoride (SF6) is an inert, heavy gas having good dielectric and arc quenching properties. SF6 is now being very widely used in electrical equipments like high voltage metal enclosed cables, high voltage switchgears, bushings and circuit breakers.

The types of SF6 circuit breaker can be broadly identified as:

- Double pressure type.
- Singly pressure puffer type.

For double pressure type, the gas from high pressure system is released into the low pressure system through a nozzle during the arc extinction processes. This design has become obsolete.

In single pressure puffer type, the gas is compressed by moving cylinder system and is released through a nozzle while extinguishing the arc. This design is most popular over wide range of voltages from 3.6 kV to 760 kV [50].

Furthermore, in both the double pressure and single pressure designs, the circuit breakers have been developed in the following two types of indoor and outdoor designs.

- Live tank design.
- Dead tank design.

In the live tank design, the interrupters are supported on porcelain insulators. Fig. 2.5 shows 72.5 kV live tank SF6 circuit breaker.

Figure 2.5 (72.5 kV) Live tank SF6 circuit breaker

While in dead tank design, interrupters installed within SF6 gas filled tank at earth potential. This configuration is used in Gas Insulated Switchgear (GIS) [50].

Figure 2.6 (72.5 kV) Dead tank SF6 circuit breaker

The major advantages and disadvantages of SF6 circuit breaker can be summarized in Table 2.1.

Table 2.1 Major advantages and disadvantages of SF6 breaker [50]

Sr. No	advantages	disadvantages
1	Has less number of interrupters per pole than the other types, as a result its less costly, maintenance free and compact.	Sealing problem arise.
2	Te gas is non-inflammable and chemically stable.	Arced SF6 gas is poisonous and should not be inhaled or let out.
3	Ample overload margin due to the superior heat transferability of SF6.	SF6 gas is sensitive to moisture.
4	The breaker is silent and doesn't make sound like ABCB during operation.	Mechanism is required for high energy level breaker.
5	Ability to interrupt different types of fault currents in excellent performance.	Special facilities are required to transfer the gas and to maintain the quality of the gas.
6	Excellent insulating and arc extinguishing medium.	
4	No over-voltages problem and no frequent contact replacement.	

2.6.4 Vacuum Circuit Breaker (VCB)

Vacuum circuit breaker is widely used in medium voltage range (1-38) kV with one interrupter per pole, and rarely used in the HV application, since it needs multi interrupter per pole and that complicates the circuit breaker, threats the durability and decreases the cost effectiveness of the breaker. A medium voltage circuit breaker is shown in Fig. 2.7.

The high speed of dielectric recovery after rapid and silent operations, suitability for repeated operation, simple operation mechanism, freedom from explosion, flexibility of design and long of life make the VCB the perfect choice in medium voltage applications.

Figure 2.7 Withdraw-able medium voltage vacuum circuit breaker

2.6.5 Testing of High Voltage AC Circuit Breaker

The tests on high voltage circuit breakers can be classified as follows:

- Development tests.
- Type tests.
- Routine tests.
- Reliability tests.
- Commissioning tests.

The development tests are carried out on components, sub-assemblies and complete circuit breaker during and after the development of the circuit breaker. The designers and research scientists verify the effect of various parameters on the behavior of circuit

breaker, by conducting development test. Development tests are not specified in the standards.

For type tests these are conducted on first few prototype circuit breakers of each type to prove the capabilities and to confirm the rated characteristics of the circuit breaker of that design. Type tests are not conducted on every circuit breaker. The tests are conducted in specially built testing laboratories. Type tests are performed as per recommendations of standards such as IEC or ANSI.

According to IEC, the type test of high voltage AC circuit breaker includes the following tests which have been summarized in Table 2.2.

Table 2.2 Summary of type tests on high voltage AC circuit breaker according to IEC standard [50]

Sr. No	Test	Remarks
1	No load mechanical operation test.	No load operations to verify speed of travel, opening time and closing time. Carried out at 85% and 110% rated voltage of shunt trip release.
2	Mechanical performance tests. (endurance tests)	1000 close-open operations.
3	Temperature rise test.	Steady temperature of conducting parts and insulating parts measured for rated continuous alternating current.
4	Dielectric test, (1.2/50) μs lightning impulse withstand and one minute power frequency voltage withstand dry and wet.	Five consecutive shots of positive and then negative polarity. One minute power frequency withstand.
5	Short time current test.	Rated short circuit current passed through closed breaker for 1 sec or 3 sec.

6	Short circuit breaking and making and braking.	At 10%, 30%, 60% and 100% rated short circuit breaking current with specified operating sequence and specified TRV (Transient Recovery Voltage).
7	Line charging current breaking tests.	Applicable for circuit breakers rated 72.5 kV and above to be used for over head lines.
8	Cable charging current breaking tests.	Applicable to circuit breaker intended for long cable network.
9	Single capacitor bank breaking tests.	Applicable for circuit breaker to be used for capacitor switching.
10	Small inductive current breaking tests. (Reactor switching)	Applicable to circuit breaker for shunt reactors, transformers and motors.
11	Out-of-phase switching.	Applicable to circuit breakers which may connect two parts made out-of-phase conditions.
12	Short line fault test.	Applicable to circuit breaker rated above 52 kV and for overhead lines. These are in addition to basic short circuit test duties.

Routine tests are also performed as per the recommendations of the standards, they are conducted on each circuit breaker in the manufacturer's premises.

Routine tests confirm the proper functioning of circuit breaker.

Reliability tests are conducted to verify the reliability of the circuit breakers under various stresses occurring in actual applications and can be conducted in specially built laboratories and also at site.

Finally, the Commissioning tests are conducted on the circuit breaker after installation at site to verify the operational and proper functioning.

CHAPTER 3

PROBLEM FORMULATION

SF6 gas is very sensitive to the EF uniformity. Therefore, our case here is how to design CB interrupting chamber with high EF uniformity in order to increase the break down voltage, i.e. we need to minimize the EF at the points which contain high field concentration (the sharp edges). Fig. 3.1 shows a schematic diagram of an SF6 circuit breaker chamber.

3.1 THE PROPOSED OBJECTIVE FUNCTION

For the breaker in Fig. 3.1, the following objective function has been proposed:

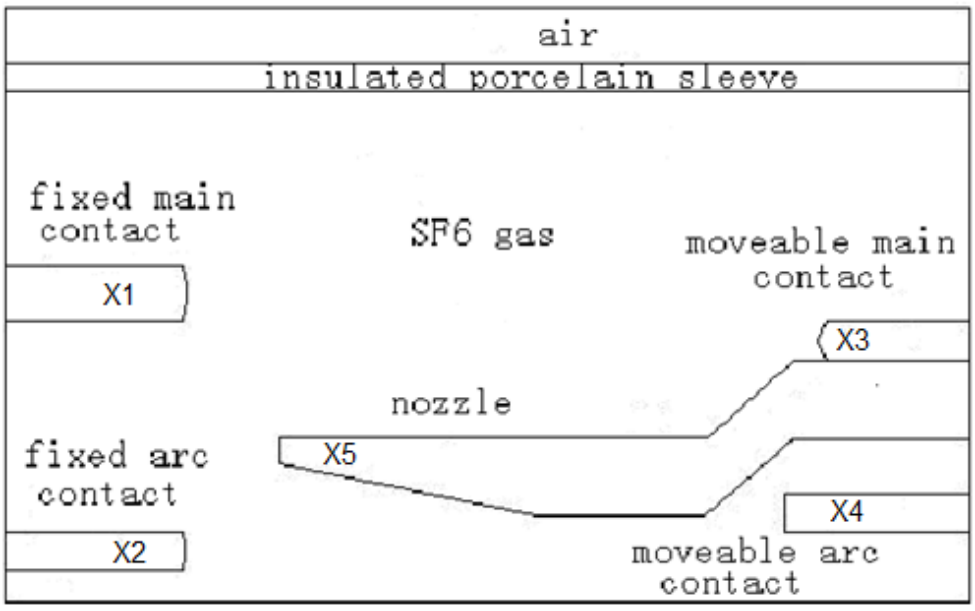

Figure 3.1 Schematic diagram of SF6 circuit breaker

$$J = Min\{Max(E)\} \tag{3.1}$$

$$E = f(x_1, x_2, x_3, x_4, x_5) \tag{3.2}$$

x_1: Fixed main contact radius (mm).

x_2: Fixed arc contact radius (mm).

x_3: Movable main contact radius (mm).

x_4: Movable arc contact radius (mm).

x_5: Nozzle radius (mm).

The variables' constraints are as follow:

$$x_{1min} \leq x_1 \leq x_{1max}$$

$$x_{2min} \leq x_2 \leq x_{2max}$$

$$x_{3min} \leq x_3 \leq x_{3max}$$

$$x_{4min} \leq x_4 \leq x_{4max}$$

$$x_{5min} \leq x_5 \leq x_{5max}$$

Since the numerical values for the constrains were not mentioned in the tested cases [1] and [43], the constrain values for the proposed optimization problem were set based on the following:

- The minimum constrains

  These values were selected based on the fact that the minimum radius which can be created between two points (A & B in Fig. 3.2) can't be less than the half of the distance (d) between the two points plus small margin (e, 0.1 mm for example).

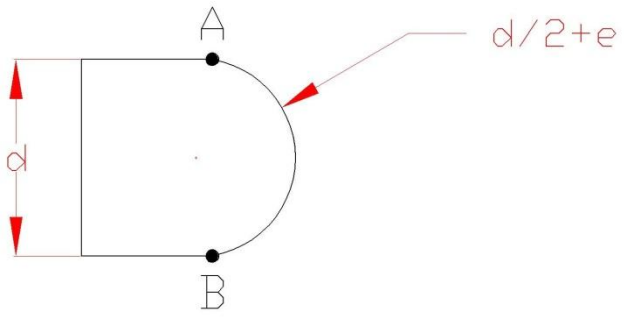

Figure 3.2 Minimum constrains explanation

- The maximum constrains

  After a increasing the radius of the arc between two points (A & B in Fig. 3.3) to a certain range, the shape of that arc will be almost flat (straight line). So a value of (30 mm) was selected as an upper limit to reduce the size of the searching domain in the two tested cases. The same is shown in Fig. 3.3.

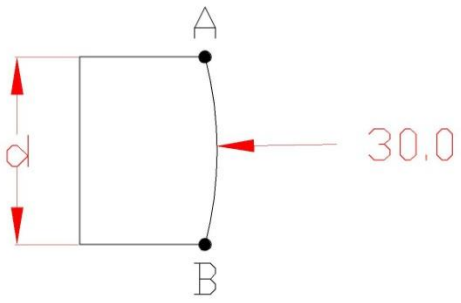

Figure 3.3 Maximum constrains explanation

The used governing equation which describes the electric field inside the HVCB chamber is given as follows:

$$\bar{E} = -\nabla V \tag{3.3}$$

Where the voltage was obtained by solving the 2D (due to the axial symmetry, special cases form Equation 2.2 and 2.1 were derived) Laplace's and Poisson's equations for the free space charge medium and medium with space charge respectively.

$$\frac{\partial^2 V}{\partial x^2} + \frac{\partial^2 V}{\partial y^2} = 0 \tag{3.4}$$

$$\frac{\partial^2 V}{\partial x^2} + \frac{\partial^2 V}{\partial y^2} = \frac{-\rho_s}{\varepsilon} \tag{3.5}$$

ANSYS calculates the electric field values described by equation (3.3) numerically (by finite element) at each node and finally we get the following vector:

$$\overline{E_\iota} = E_x \hat{a}_x + E_y \hat{a}_y \tag{3.6}$$

Where (i) the node number. From this expression we can get easily the magnitude of the electric field at that node:

$$\overline{|E_\iota|} = \sqrt{{E_x}^2 + {E_y}^2} \tag{3.7}$$

3.2 FINITE ELEMENT METHOD (FEM)

3.2.1 Basic Concept

The finite element method is based on the idea of building complicated object with simple blocks, or dividing a complicated object into small and manageable pieces. Application of this simple idea can be found everywhere in everyday life, as well as in the engineering [51].

A simple example of this technique is the approximation of the area of a circle, Fig. 3.4 shows that.

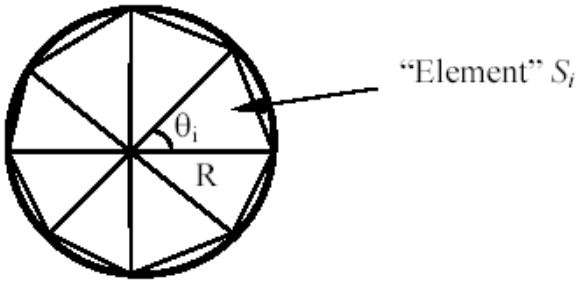

Figure 3.4 circle approximation

Area of one triangle:

$$S_i = \frac{1}{2} R^2 \sin \theta_i \tag{3.8}$$

Area of the circle:

$$S_N = \sum_{i=1}^{N} S_i = \frac{1}{2} R^2 N \sin\left(\frac{2\pi}{N}\right) \tag{3.9}$$

$$S_N = \pi R^2 \; as \;\; N \to \infty$$

Where N is the total number of triangles (elements).

The applications of FE in engineering are as follows:

- Mechanical/ Aerospace/ Civil/ Automobile engineering.
- Structure analysis (static/dynamic, linear/nonlinear).
- Thermal/ fluid flows.
- Electromagnetic.
- Geomechanics.
- Biomechanics.

The computer implementation of the FE normally done according to the following steps:

1- Preprocessing (build FE model, loads and constrains).

The user handles this step by selecting the analysis type, element type and material properties.

2- FE solver (assemble and solve the system of equation).

The software handles this step by making the nodes, building the elements, applying the boundary conditions and finally solving the problem (the set of equations).

3- Postprossering (sort and display the results).

The user handles this step.

FE can be classified to three types:

- 1-D (line) element.
- 2-D (plane) element.
- 3-D (solid) element.

The major advantages and disadvantages of FE method are summarized in Table 3.1.

Table 3.1 Major advantages and disadvantages of FE method [52]

Sr. No	advantages	disadvantages
1	Can readily handle very complex geometry.	A general closed-form solution which would permit one to examine system response to changes in various parameters is not produced.
2	Can handle a wide variety of engineering problems.	The FEM obtains only "approximate" solutions.
3	Can handle complex restraints.	The FEM has "inherent" errors.
4	Can handle complex loading.	Mistakes by users can be fatal.

3.2.2 FE Mathematical Formulation

The first concern is with the element equations [53]. Essentially there are two types: triangles and quadrilaterals.

Triangular elements use the linear polynomial:

$$u(x,y) = a_0 + a_1 x + a_2 y \tag{3.10}$$

Where $u(x,y)$ is the dependent variable (the voltage in electrostatic problems), the a_i 's are coefficients, and x and y are the independent variables. This function must pass through the values of $u(x,y)$ at the triangle's nodes (x_1,y_1), (x_2,y_2) and (x_3,y_3). Therefore,

$$u_1 = a_0 + a_1x_1 + a_2y_1 \tag{3.11}$$

$$u_2 = a_0 + a_1x_2 + a_2y_2 \tag{3.12}$$

$$u_3 = a_0 + a_1x_3 + a_2y_3 \tag{3.13}$$

Solving for a_0, a_1 and a_2 we have that

$$a_0 = [u_1(x_2y_3 - x_3y_2) + u_2(x_3y_1 - x_1y_3) + u_3(x_1y_2 - x_2y_1)]/A \tag{3.14}$$

$$a_1 = [u_1(y_2 - y_3) + u_2(y_3 - y_1) + u_3(y_1 - y_2)]/A \tag{3.15}$$

$$a_2 = [u_1(x_3 - x_2) + u_2(x_1 - x_3) + u_3(x_2 - x_1)]/A \tag{3.16}$$

Where A is the area of the triangular element

$$A = \frac{1}{2}[(x_2y_3 - x_3y_2) + (x_3y_1 - x_1y_3) + (x_1y_2 - x_2y_1)] \tag{3.17}$$

Collecting terms, the result can be expressed as

$$u(x,y) = N_1u_1 + N_2u_2 + N_3u_3 \tag{3.18}$$

Where

$$N_1 = [(x_2y_3 - x_3y_2) + (y_2 - y_1)x + (x_3 - x_2)y]/(2A) \quad (3.19)$$

$$N_2 = [(x_3y_1 - x_1y_3) + (y_3 - y_1)x + (x_1 - x_3)y]/(2A) \quad (3.20)$$

$$N_3 = [(x_1y_2 - x_2y_1) + (y_1 - y_2)x + (x_2 - x_1)y]/(2A) \quad (3.21)$$

Fig. 3.3 shows sample triangular element.

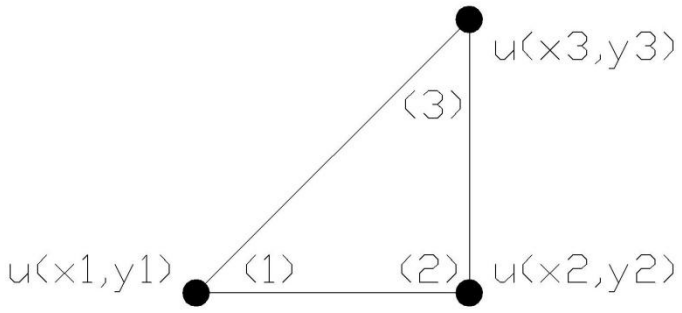

Figure 3.5 Sample triangular element

On the other hand, rectangular elements use the interpolation formula:

$$u(x, y) = N_1u_1 + N_2u_2 + N_3u_3 \quad (3.22)$$

Applying the same procedure as before, we have that

$$N_1 = (b - x)(a - y)/(4ab) \quad (3.23)$$

$$N_2 = (b + x)(a - y)/(4ab) \quad (3.24)$$

$$N_3 = (b + x)(a + y)/(4ab) \tag{3.25}$$

$$N_4 = (b - x)(a + y)/(4ab) \tag{3.26}$$

Where $2b$ and $2a$ are the length and height of the element respectively. The same is illustrated in Fig. 3.4.

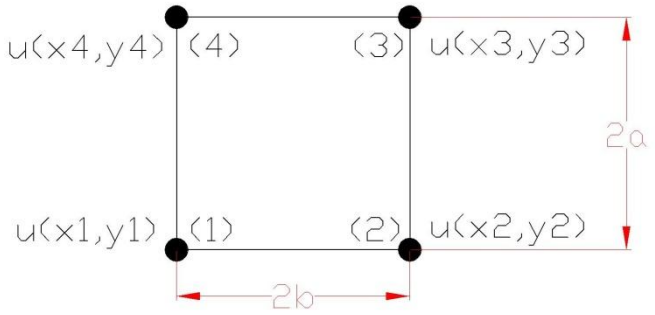

Figure 3.6 Sample rectangular element

To formulate the FE for linear triangular element, we have

$$[K^e][u^e] = \iint_{\Omega^e} \left(\frac{\partial w}{\partial x}\frac{\partial u}{\partial x} + \frac{\partial w}{\partial y}\frac{\partial u}{\partial y}\right) dxdy \tag{3.27}$$

Where $w(x, y)$ is a weighting function.

$$[K^e][u^e] = \left\{\iint_{\Omega^e} \sum_{n=1}^{3} \left[\left(\frac{\partial N_n}{\partial x}\right)^2 + \left(\frac{\partial N_n}{\partial y}\right)^2\right] dxdy\right\} u^e \tag{3.28}$$

Where Ω^e is the element's domain. Upon substituting for N_1, $N_2$and N_3 we have and carrying out the integration,

$$[K^e] = \begin{pmatrix} k_{11} & k_{12} & k_{13} \\ k_{21} & k_{22} & k_{23} \\ k_{31} & k_{32} & k_{33} \end{pmatrix} \tag{3.29}$$

$$k_{11} = [(x_3 - x_2)^2 + (y_2 - y_3)^2]/(4A) \tag{3.30}$$

$$k_{12} = [(x_3 - x_2)(x_1 - x_3) + (y_2 - y_3)(y_3 - y_1)]/(4A) \tag{3.31}$$

$$k_{13} = [(x_3 - x_2)(x_2 - x_1) + (y_2 - y_3)(y_1 - y_2)]/(4A) \tag{3.32}$$

$$k_{21} = k_{12} \tag{3.33}$$

$$k_{22} = [(x_1 - x_3)^2 + (y_3 - y_1)^2]/(4A) \tag{3.34}$$

$$k_{23} = [(x_1 - x_3)(x_2 - x_1) + (y_3 - y_1)(y_1 - y_2)]/(4A) \tag{3.35}$$

$$k_{31} = k_{13} \tag{3.36}$$

$$k_{32} = k_{23} \tag{3.37}$$

$$k_{33} = [(x_2 - x_1)^2 + (y_1 - y_2)^2]/(4A) \tag{3.38}$$

In case of a rectangular element, we now have

$$[K^e][u^e] = \left\{ \iint_{\Omega^e} \sum_{n=1}^{4} \left[\left(\frac{\partial N_n}{\partial x} \right)^2 + \left(\frac{\partial N_n}{\partial y} \right)^2 \right] dxdy \right\} u^e \tag{3.39}$$

Carrying out the integration,

$$[K^e] = \begin{pmatrix} k_{11} & k_{12} & k_{13} & k_{14} \\ k_{21} & k_{22} & k_{23} & k_{24} \\ k_{31} & k_{32} & k_{33} & k_{34} \\ k_{41} & k_{42} & k_{43} & k_{44} \end{pmatrix} \tag{3.40}$$

Where

$$k_{11} = \frac{b^2+a^2}{3ab}, \qquad k_{12} = \frac{b^2-2a^2}{6ab} \tag{3.41}$$

$$k_{13} = -\frac{b^2+a^2}{6ab}, \qquad k_{14} = \frac{a^2-2b^2}{6ab} \tag{3.42}$$

$$k_{22} = k_{11}, \qquad k_{23} = k_{14}, \qquad k_{24} = k_{13} \tag{3.43}$$

$$k_{33} = k_{11}, \qquad k_{34} = k_{12}, \qquad k_{44} = k_{11} \tag{3.44}$$

In the triangular element as well as the rectangular one, once the $[K^e]$ matrix evaluated from the geometry itself and the boundary conditions at certain points ($u_{1,}u_2 \ldots etc$) are known, the value of $u(x,y)$ will be available at all the available node by solving the following equation:

$$[u^e] = [K^e]^{-1}[F^e] \tag{3.45}$$

Where F^e is the action (charge in electrostatic problems) at that element.

CHAPTER 4

PROPOSED SOLUTION ALGORITHMS

After formulating the electric field problem in CB chamber as an optimization problem, the following step by step algorithm provides solution for such a non-linear electric field, the complete code has been written in the APDL language and the code was fully compiled by ANSYS software.

The general skeleton of the algorithm use either the (PS) or (SA) artificial intelligence techniques.

Step 1: the first macro which contains the optimization codes runs and sends the candidates (the optimized parameters) each time to another macro to get the objective/cost function value (maximum electric field) for each one, and finally we ends up with the best candidate.

Step 2: the second macro receives the candidates from the optimization macro, and calculates the objective/cost function (maximum electric field) accordingly and sends the solution back to the fist macro.

The flowchart that summarizes the above mentioned steps is given by Fig. 4.1.

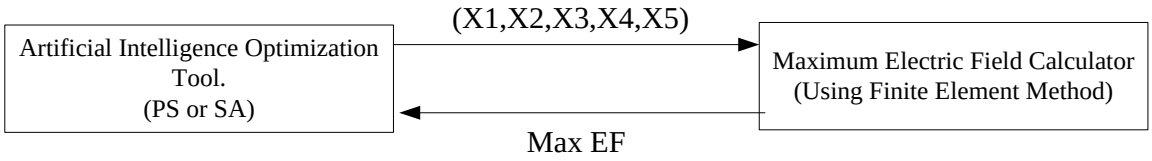

Figure 4.1 Skeleton flowchart for the used optimization algorithms

4.1 PARTICLE SWARM ALGORITHM (PS)

In this section the (PS) optimization technique [54-57] will be illustrated by considering the CB chamber problem as an example.

The basic elements of (PS) technique are briefly stated and defined as follows: -

Particles:

The optimized parameters (x_1, x_2, x_3, x_4 & x_5).

Population:

The population of the optimized parameters has been created (random candidates within the search space) inside the following matrices (X1P, X2P, X3P, X4P and X5P).

Particles velocity:

The particles velocity of the optimized parameters has been created inside the following matrices (X1V, X2V, X3V, X4V and X5V).

Inertial weight:

It is a control parameter or matrix (X1SOLDEF for example) that is used to control the impact of the previous velocities on the current velocity, in our case the difference between the global best solution (BESTCHILD) and the initial parameters (X1P matrix for example) multiplied by random number (between zero and one) has been used as an inertia weight.

Individual best:

The parameter (JBEST) has been used as individual best locater to save the best solution which obtained from each generation.

Global best:

The parameter (BESTCHILD) has been used as global best locater to save the best solution which obtained from all the generations.

Stopping criteria:

The number of iteration (N=50) has been used as a termination condition.

The (PS) technique can be described in the following steps:

Step 1: (initialization)

Generate randomly (N=50) particles within the search space for each parameter and save them inside the matrices (X1P, X2P, X3P, X4P and X5P).

Similarly, generate randomly initial velocities of all particles and save them inside the matrices (X1V, X2V, X3V, X4V and X5V), based on maximum and minimum value for each parameter and the population size.

Each particle in the initial population is evaluated using the objective function, Search for the best value of the objective function and save it inside the parameter (JBEST).

Step 2: (time updating)

Update the time counter N=N+1.

Step 3: (weight updating)

Update the inertia weight.

Step 4: (velocity updating)

Using the global best (BESTCHILD) and individual best (JBEST) to update the velocity for each parameters.

Step 5: (position updating)

Based on the updated velocities, each particle changes its position by adding the inertia weight (X1SOLDEF for example) to the initial position (X1P for example).

Step 6: (individual best updating)

Each particle is evaluated according to the updating position, then the individual best (JBEST) is updating by selecting the one who has the minimum objective (since this case is a minimization problem) according to the following statement:

JBEST=Min (OBJ).

Step 7: (global best updating)

Search for the minimum objectives (BESTCHILD) between all the individual best (OBJN) by implementing the following statement:

If {OBJN (I) < BESTCHILD} then {BESTCHILD= OBJN (I)}.

Step 8: (stopping criteria)

Stop when the number of iteration (N=50) is reached.

The flowchart that summarizes the above mentioned steps is given by Fig. 4.2

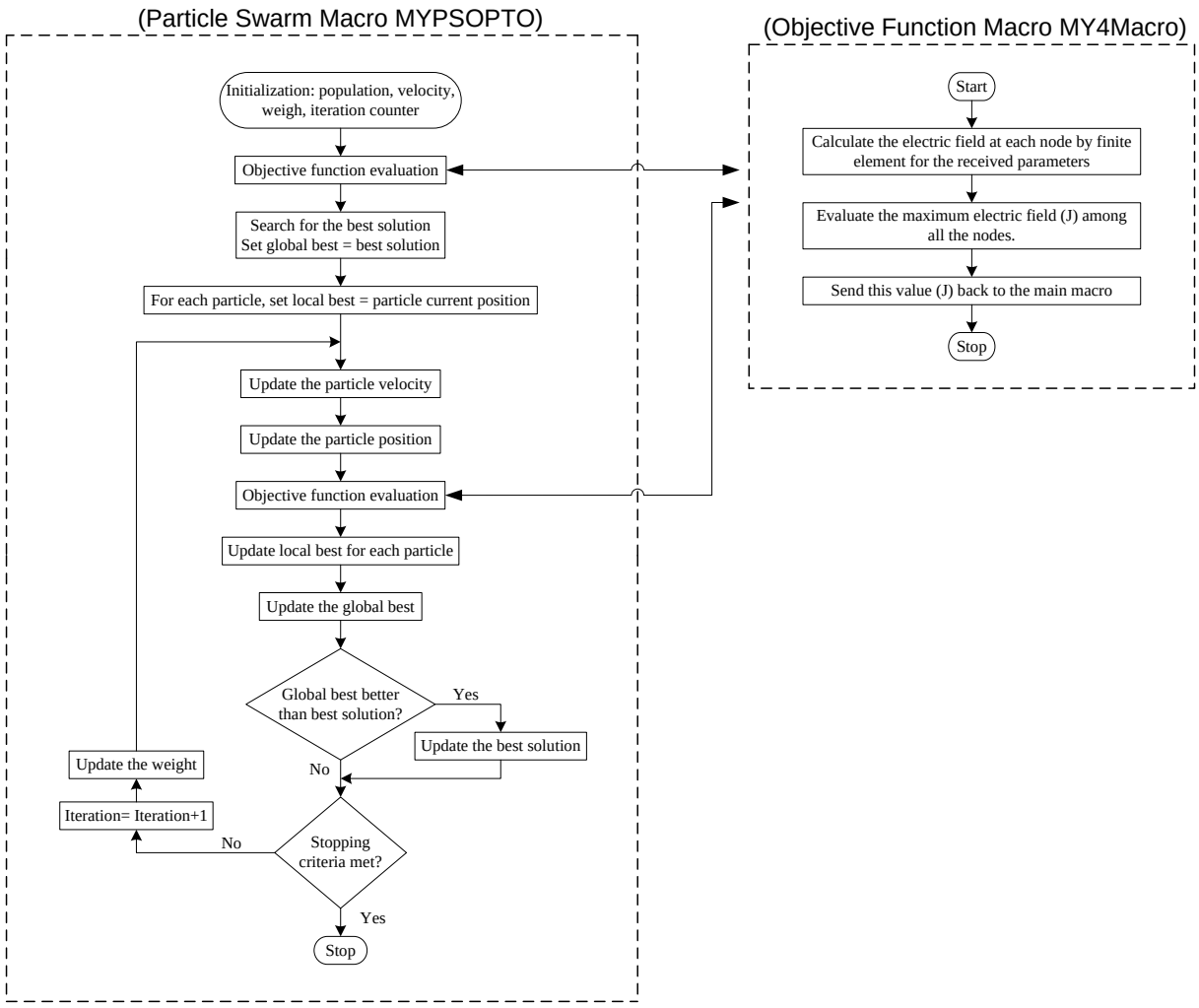

Figure 4.2 The used (PS) algorithm

4.2 SIMULATED ANNEALING ALGORITHM (SA)

In this section the (SA) optimization technique [58-59] will be illustrated by considering the CB chamber problem as an example.

The basic elements of (SA) technique are briefly stated and defined as follows: -

Current, trial and best solutions:

These solutions are sets of the optimized parameter values at any iteration, the matrices which contains the above solutions are JT, OBJ and Min (JT) respectively.

Acceptance criterion:

At any iteration, the trial solution can be accepted as the current solution if it meets one of the following criteria:

I. J (x_{trial}) < J (x_{current}).

II. J (x_{trial}) > J (x_{current}) and exp (-[J (x_{trial}) - J (x_{current})] / C_{p}) > rand (0, 1).

Here, rand (0, 1) is a random number with domain [0, 1] and J (x_{trial}) and J (x_{current}) are the objective function values associated with x_{trial} and x_{current} respectively, C_{p} is a control parameter.

Criterion (II) indicates that the trial solution is not necessarily rejected if its objective function is not as good as that of the current solution with hoping that a much better solution becomes reachable.

Acceptance ratio:

At a given value of C_{p}, a N trial solutions can be randomly generated. Based on the acceptance criterion, an N_2 of these solutions can be accepted. The acceptance ratio is defined as N_2/N.

Cooling schedule:

It specifies a set of parameters that governs the convergence of the algorithm. This set includes an initial value of control parameter C_{p0}, a decrement function for decreasing the

value of C_p, and a finite number of iterations or transitions at each value of C_p, i.e. the length of each homogeneous Markov chain.

The initial value of C_p should be large enough to allow virtually all transitions to be accepted. However, this can be achieved by starting off at a small value of C_{p0} (it's considered as 0.01) and multiplying it with a constant ALFA larger than 1 (it's considered as 1.3), i.e. (C_p= ALFA x C_p). This process continues until the acceptance ratio is close to 1. This is equivalent to heating up process in physical systems. The decrement function for decreasing the value of C_p is given by (C_p= BETA x C_p) where BETA is a constant smaller than but close to 1 (it's considered as 0.8).

Equilibrium condition:

It occurs when the current solution does not change for a certain number of iterations at a given value of C_p. It can be achieved by generating a large number of transitions at that value.

Stopping criteria:

These are the conditions under which the search process will terminate. In this study, the search will terminate if the number of heating and cooling process reaches the maximum allowable number.

The general algorithm of (SA) technique can be described in steps as follows:

Step 1:

Set the initial value of C_{p0} and randomly generate an initial solution x_{trial} and calculate its objective function. Set this solution as the current solution as well as the best solution, i.e. $x_{trial} = x_{current} = x_{best}$.

Step 2:

Randomly generate an N of trial solutions in the neighborhood of the current solution.

Step 3:

Check the acceptance criterion of these trial solutions and calculate the acceptance ratio. If acceptance ratio is close to 1 go to step 4; else set (C_p= ALFA x C_p), and go back to step 2.

Step 4:

Generate a trial solution x_{trial}. If x_{trial} satisfies the acceptance criterion set $x_{current} = x_{trial}$, J($x_{current}$) = J(x_{trial}), and go to step 5; else go to step 3.

Step 5:

Check the equilibrium condition. If it is satisfied go to step 6; else go to step 4.

Step 6:

Check the stopping criteria. If one of them is satisfied then stop; else set (C_p= BETA x C_p) and go back to Step 4.

The flowchart that summarizes the above mentioned steps is given by Fig. 4.3

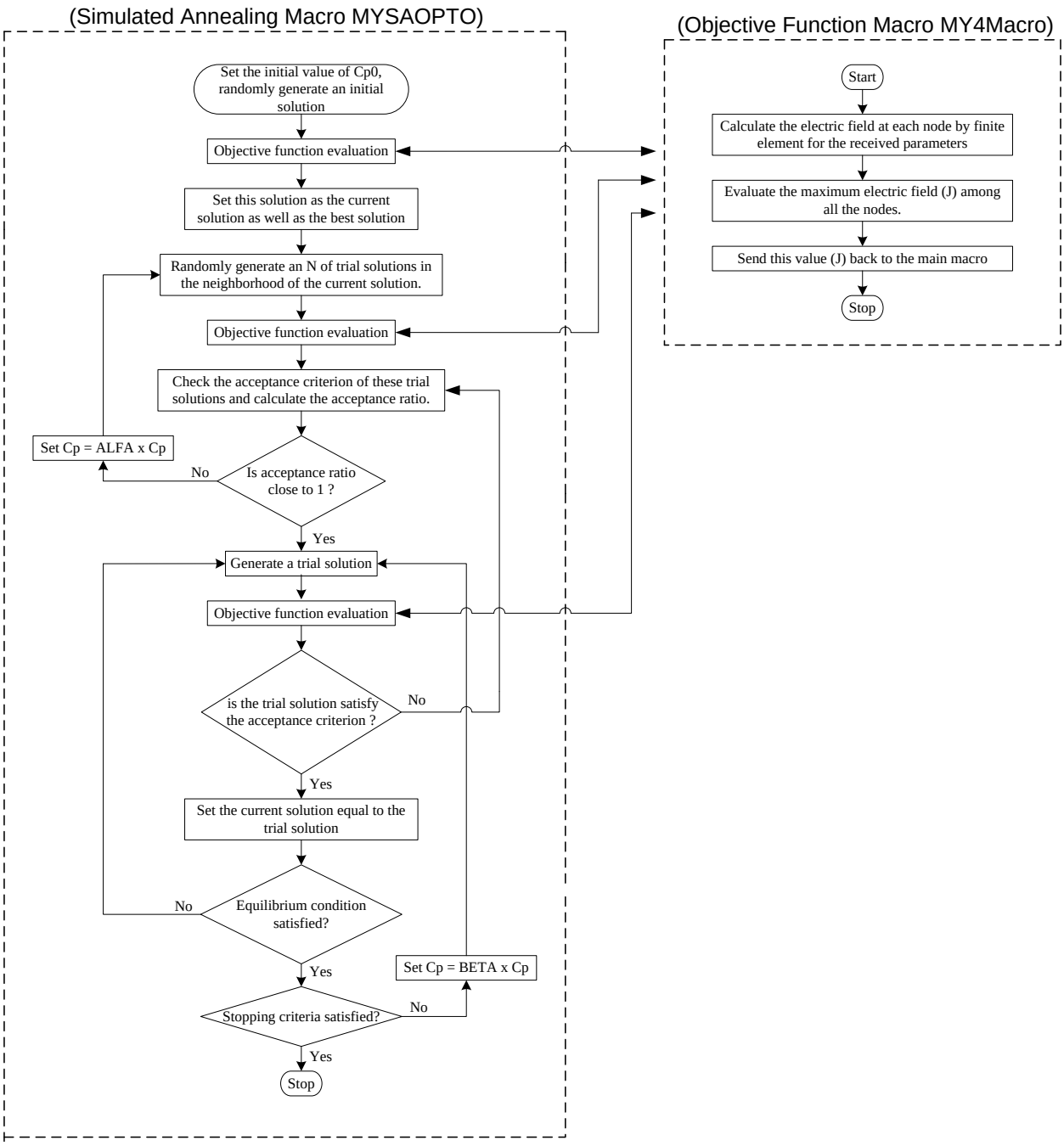

Figure 4.3 The used (SA) algorithm

CHAPTER 5

SIMULATION RESULTS & DISCUSSION

The effectiveness of the proposed optimization algorithm has been demonstrated by comparing the current optimized results with two different CB designs reported in the literature [1] and [43]. The first CB is rated 252 kV and the other is rated at 550 kV.

5.1 Case 1: 252 kV SF6 CB [1]

In order to test the performance of the proposed solution algorithm, a benchmark CB chamber optimization problem [1] has been used.

5.1.1 Optimizing Electric Field Using Laplace's Equation.

The parameters, constrains of that parameters and geometry of the tested 252 kV CB are given in Table 5.1, Table 5.2 and Fig. 5.1 respectively.

Table 5.1 Parameters of the tested CB

Fixed main contact radius (mm)	Fixed arc contact radius (mm)	Movable main contact radius (mm)	Movable arc contact radius (mm)	Nozzle radius (mm)
$[x_1]$	$[x_2]$	$[x_3]$	$[x_4]$	$[x_5]$
13.526	14.651	17.872	6.046	11.458

Table 5.2 The optimized parameters constrains'

Constrains range	Fixed main contact radius (mm)	Fixed arc contact radius (mm)	Movable main contact radius (mm)	Movable arc contact radius (mm)	Nozzle radius (mm)
	$[x_1]$	$[x_2]$	$[x_3]$	$[x_4]$	$[x_5]$
Minimum	7.6	5.1	7.6	5.1	4.1
Maximum	30	30	30	30	30

It’s worth to mention that all minimum values were calculated as follows:

For example for x_1 it is from (15/2 + 0.1 = 7.6)

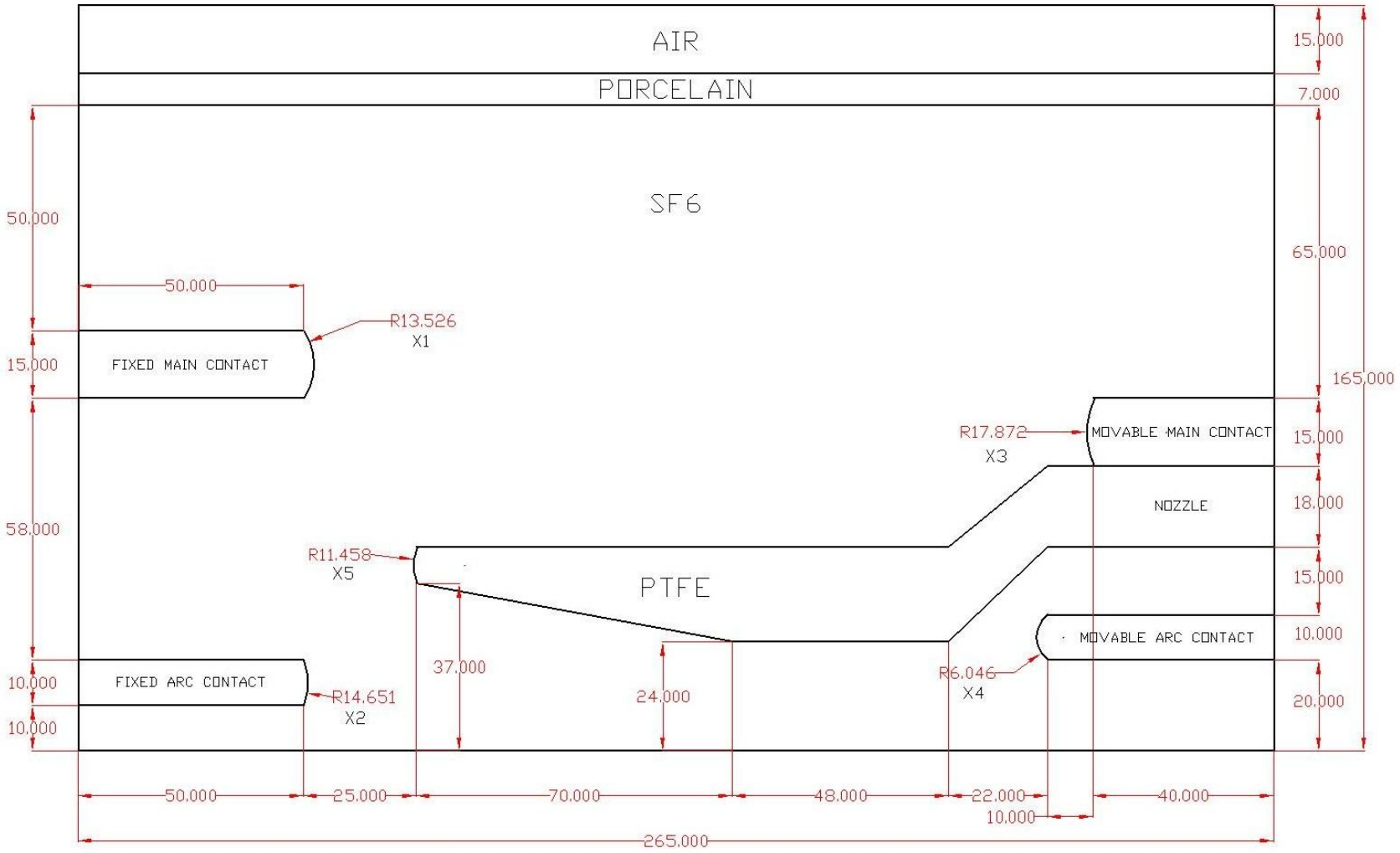

Figure 5.1 Non-optimized chamber geometry

For comparison purposes, the governing equation used in reference [1] has been used; i.e. Laplace's equation is used. The finite element grid for the initial circuit breaker chamber is shown in Fig. 5.2. The number is node is 1692.

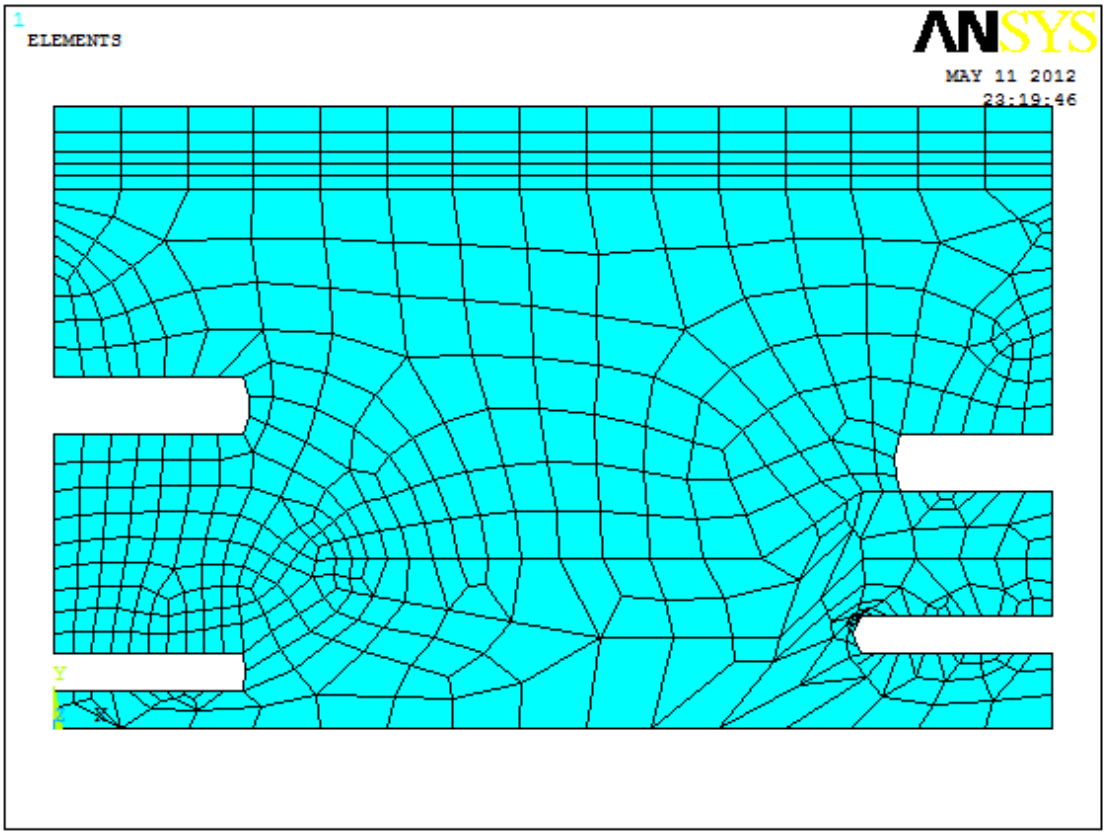

Figure 5.2 The finite element grid for the initial circuit breaker chamber

The proposed ANSYS-PS or ANSYS-SA algorithms optimized parameters as well the parameters using the non optimized and previous work reported in the literature [1] are summarized in Table 5.3.

.

Table 5.3 Maximum electric field strength for different contacts and nozzle radius

The used optimization technique	Fixed main contact radius (mm)	Fixed arc contact radius (mm)	Movable main contact radius (mm)	Movable arc contact radius (mm)	Nozzle radius (mm)	Maximum electric field (V/mm) Objective	Maximum electric field reduction (%)
	$[x_1]$	$[x_2]$	$[x_3]$	$[x_4]$	$[x_5]$	$[J]$	
(None) Initial solution	13.526	14.651	17.872	6.046	11.458	4636.61	0.0
(Particle Swarm) solution	23.316	22.57	23.316	22.57	22.272	3292.26	28.99
(Simulated Annealing) solution	22.26	21.396	22.26	21.396	21.051	3331.37	28.15
(Literature [1]) solution	17.708	11.858	10.820	15.386	13.063	4295.21	7.36

It is quite clear that the two proposed algorithms (PS) and (SA) outperform the optimization method reported before [1]. The (PS) electric field reduction reaches (28.99%), while the (SA) electric field reduction reaches (28.15%).

This is a very high reduction when compared to the method in the literature (7.36%) reduction.

The schematic diagram for the non-optimized geometry, the electric field contour and vector plotting are shown in Fig. 5.1, Fig 5.3 and Fig 5.4 respectively.

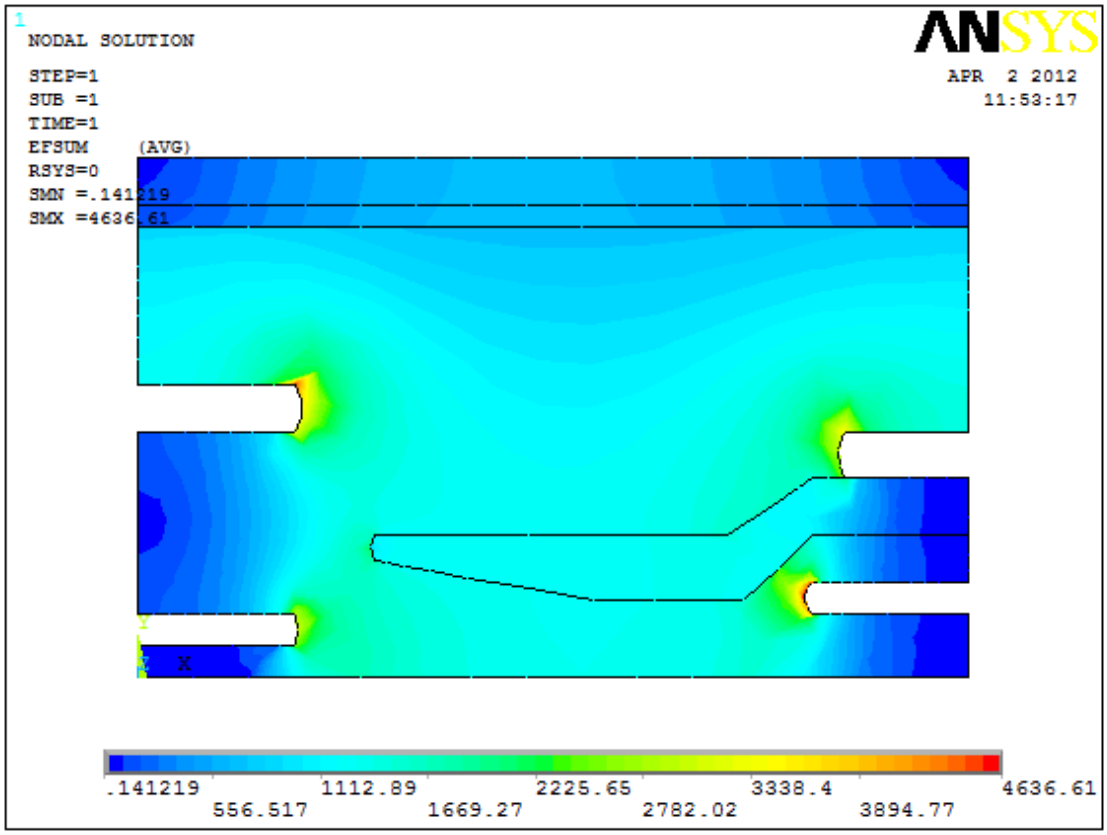

Figure 5.3 Electric field contour for the non-optimized geometry

As shown in the above figure, the maximum electric field obtained by solving the non-optimized geometry is (4636.61 V/mm) at the movable arc contact.

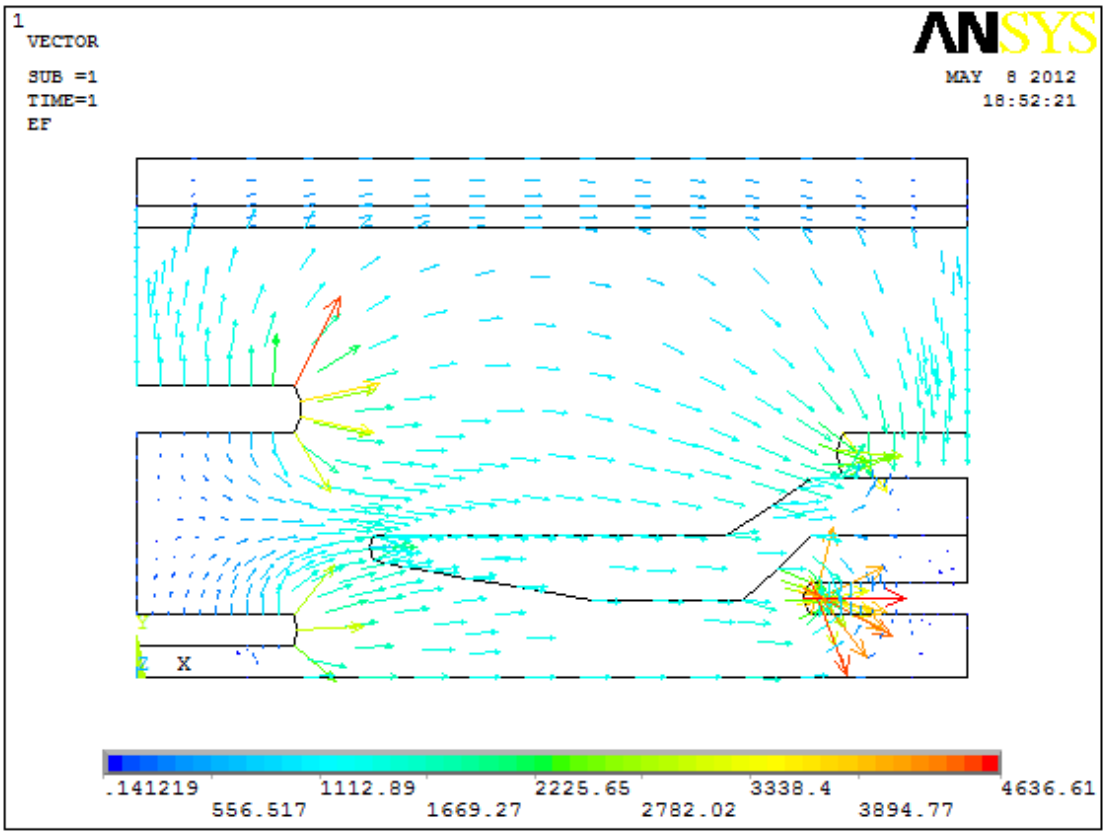

Figure 5.4 Electric field vector for the non-optimized geometry

On the other hand, Fig. 5.5, Fig 5.6 and Fig 5.7 show schematic diagram for the optimized geometry, electric field contour and field plotting for the (PS) optimized geometry respectively.

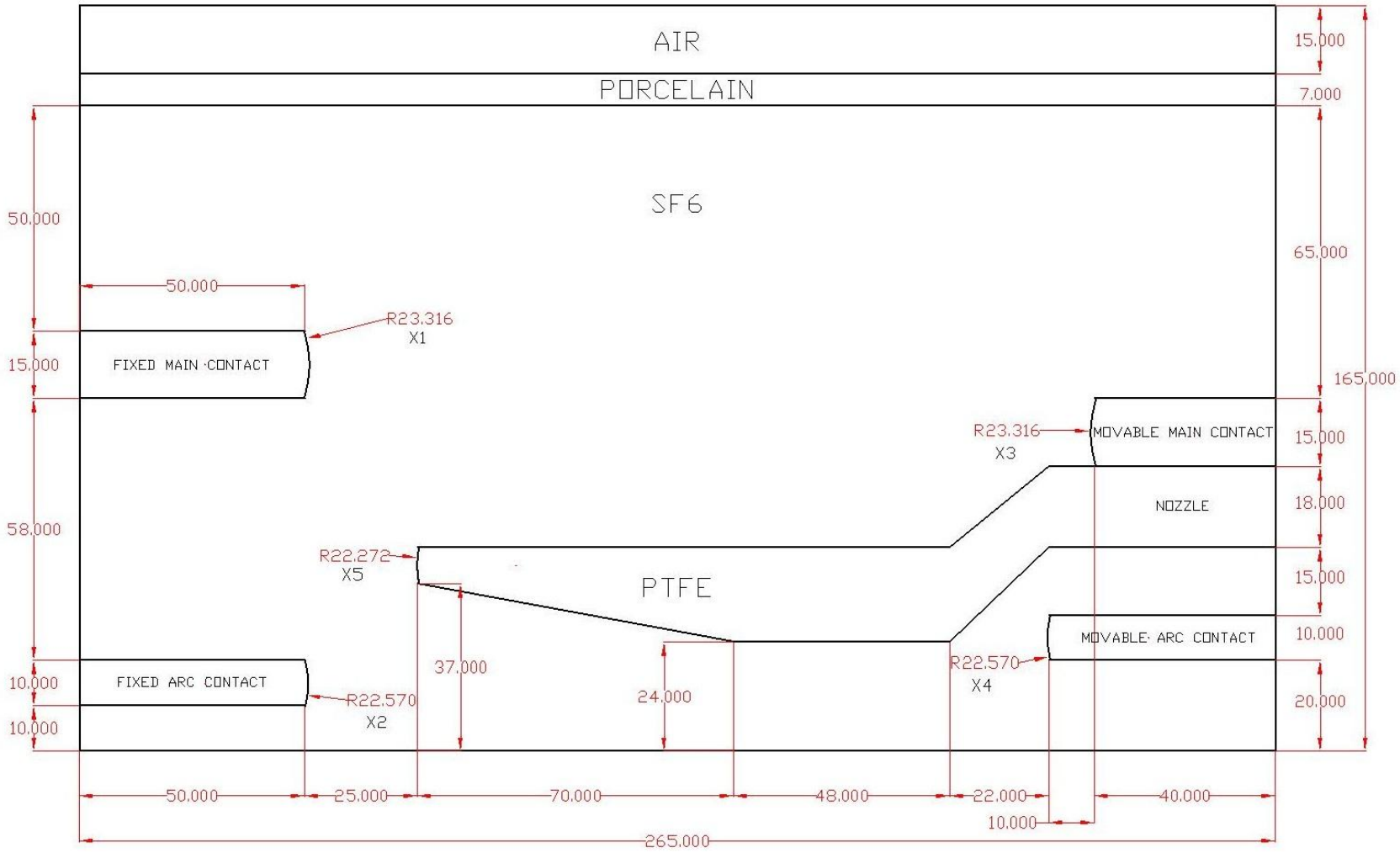

Figure 5.5 PS optimized chamber geometry

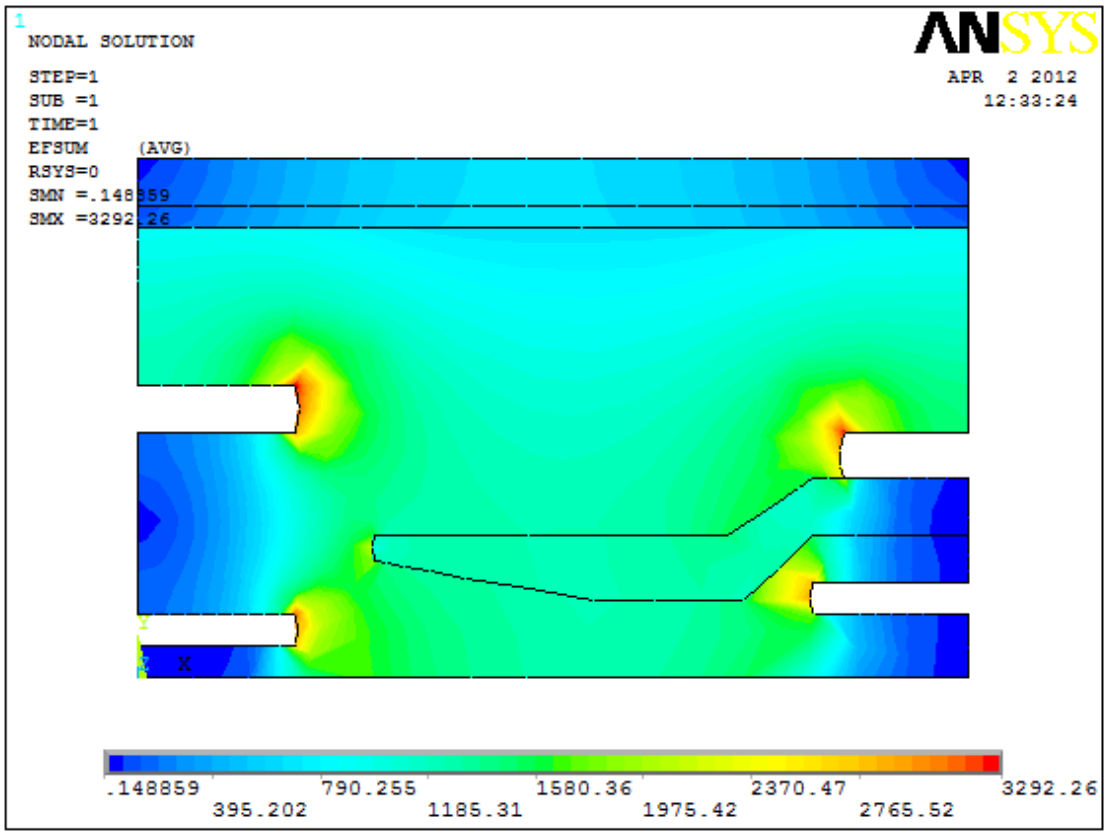

Figure 5.6 Electric field contour for (PS) optimized geometry

It is quite clear from Fig. 5.6 that the maximum electric field obtained by solving the (PS) optimized geometry is (3292.26 V/mm) at the movable arc contact. This is a reduction of 28.99% from the non optimized geometry value.

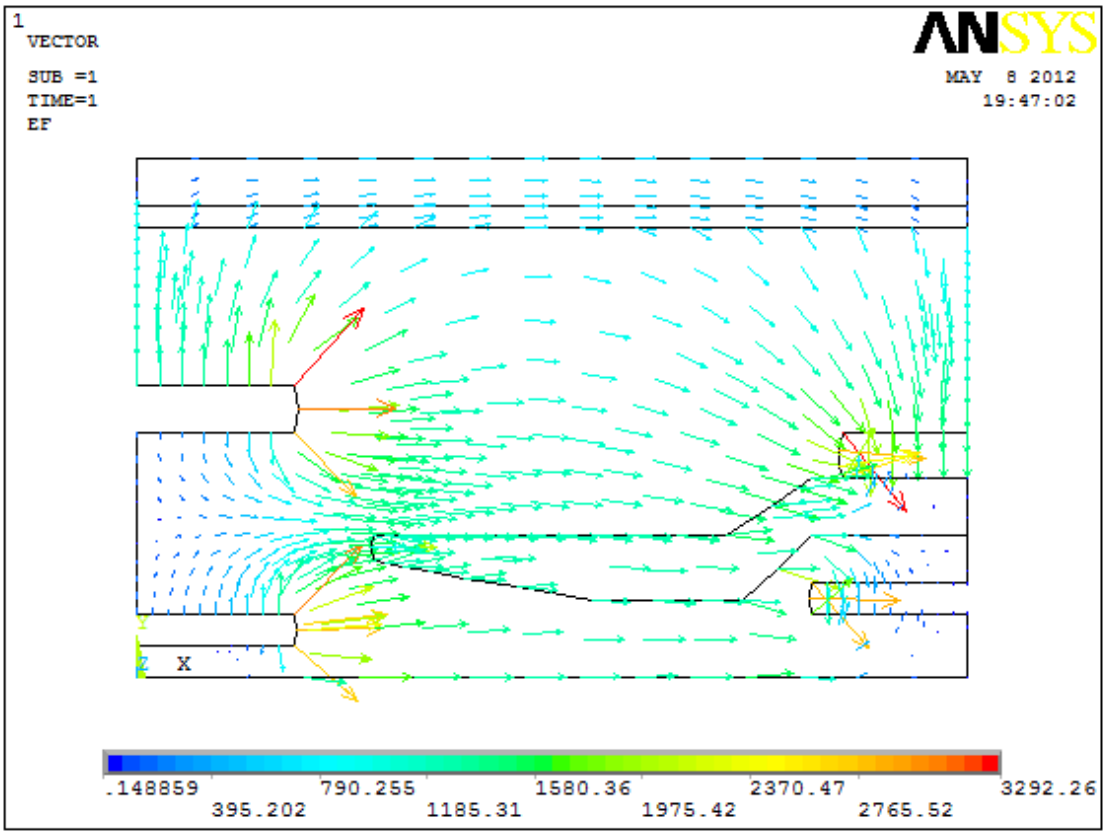

Figure 5.7 Electric field vector for (PS) optimized geometry

The same initial geometry was optimized to minimize the maximum electric field using (SA) algorithm. Fig. 5.8, Fig 5.9 and Fig 5.10 show schematic diagram for the optimized geometry, electric field contour and field plotting for the (SA) optimized geometry respectively.

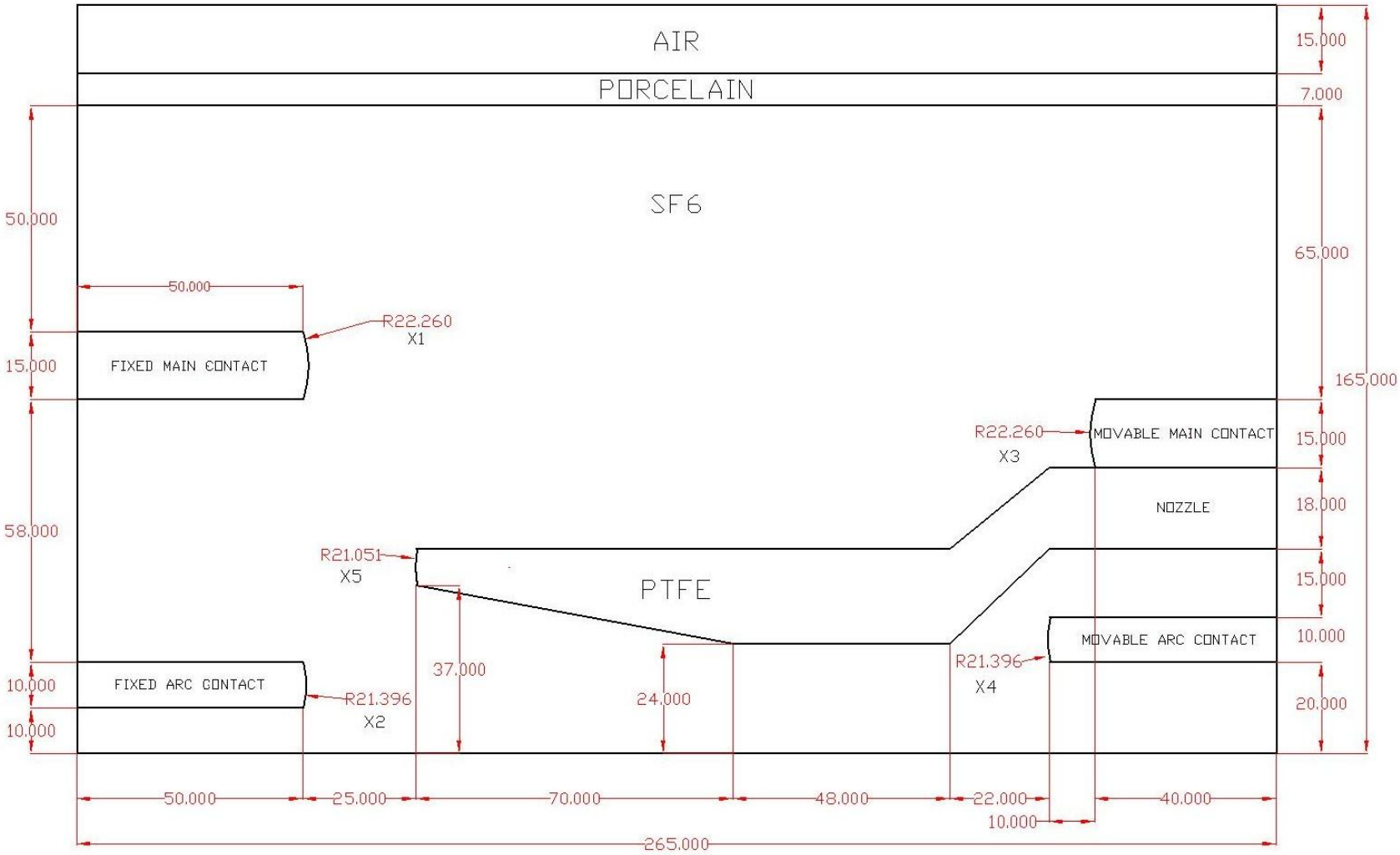

Figure 5.8 SA optimized chamber geometry

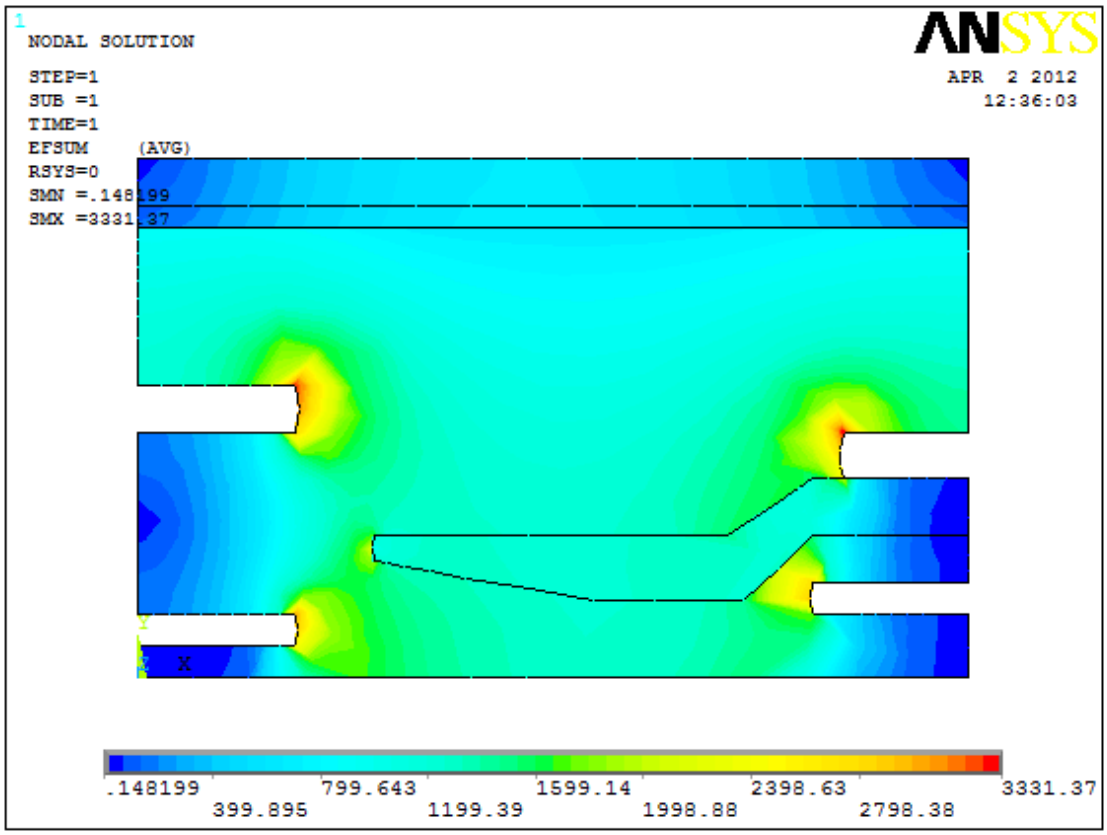

Figure 5.9 Electric field contour for the (SA) optimized geometry

As shown in the above figure, the maximum electric field obtained by solving the (SA) optimized geometry is (3331.37 V/mm) at the movable main contact. This is a reduction of 28.15% from the non optimized geometry value.

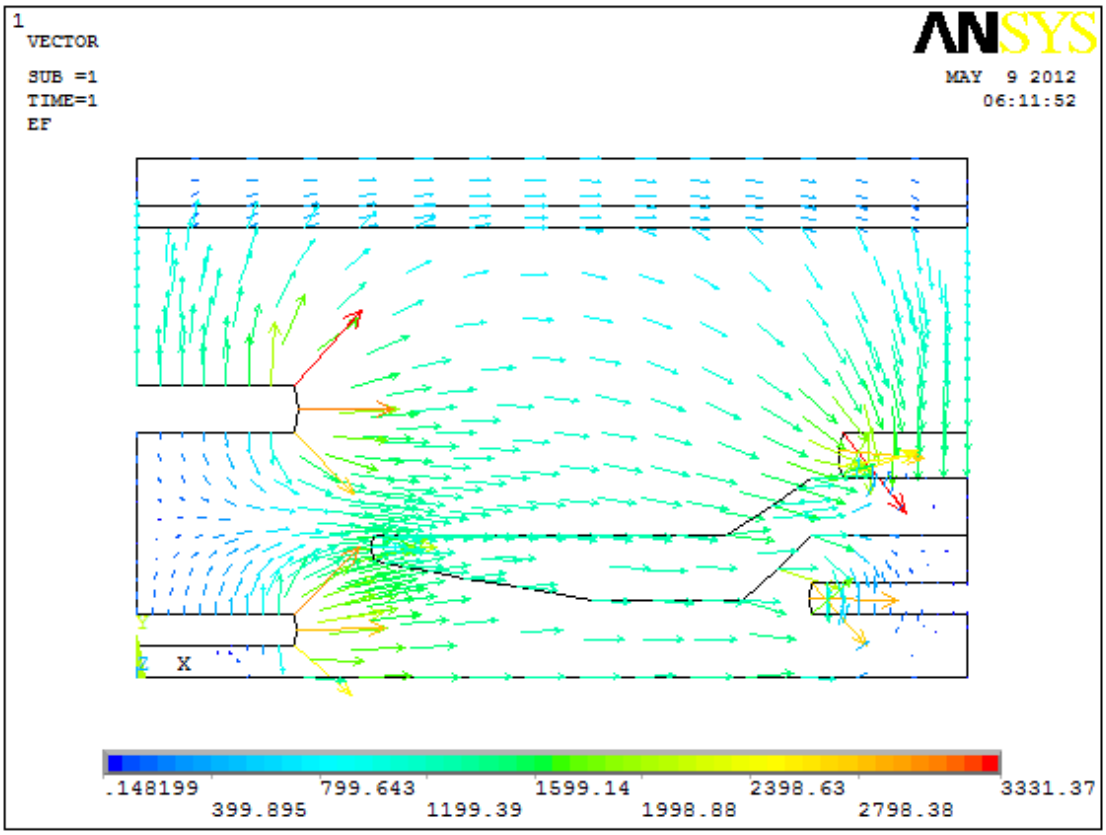

Figure 5.10 Electric field vector for the (SA) optimized geometry

Finally, the results which have been reported in the literature [1] were regenerated to compare the effectiveness of the used methods. Schematic diagram for the optimized geometry by using the built-in optimization tool in ANASYS, the electric field contour and vector plotting for the same are shown in Fig. 5.11, Fig. 5.12 and Fig 5.13 respectively.

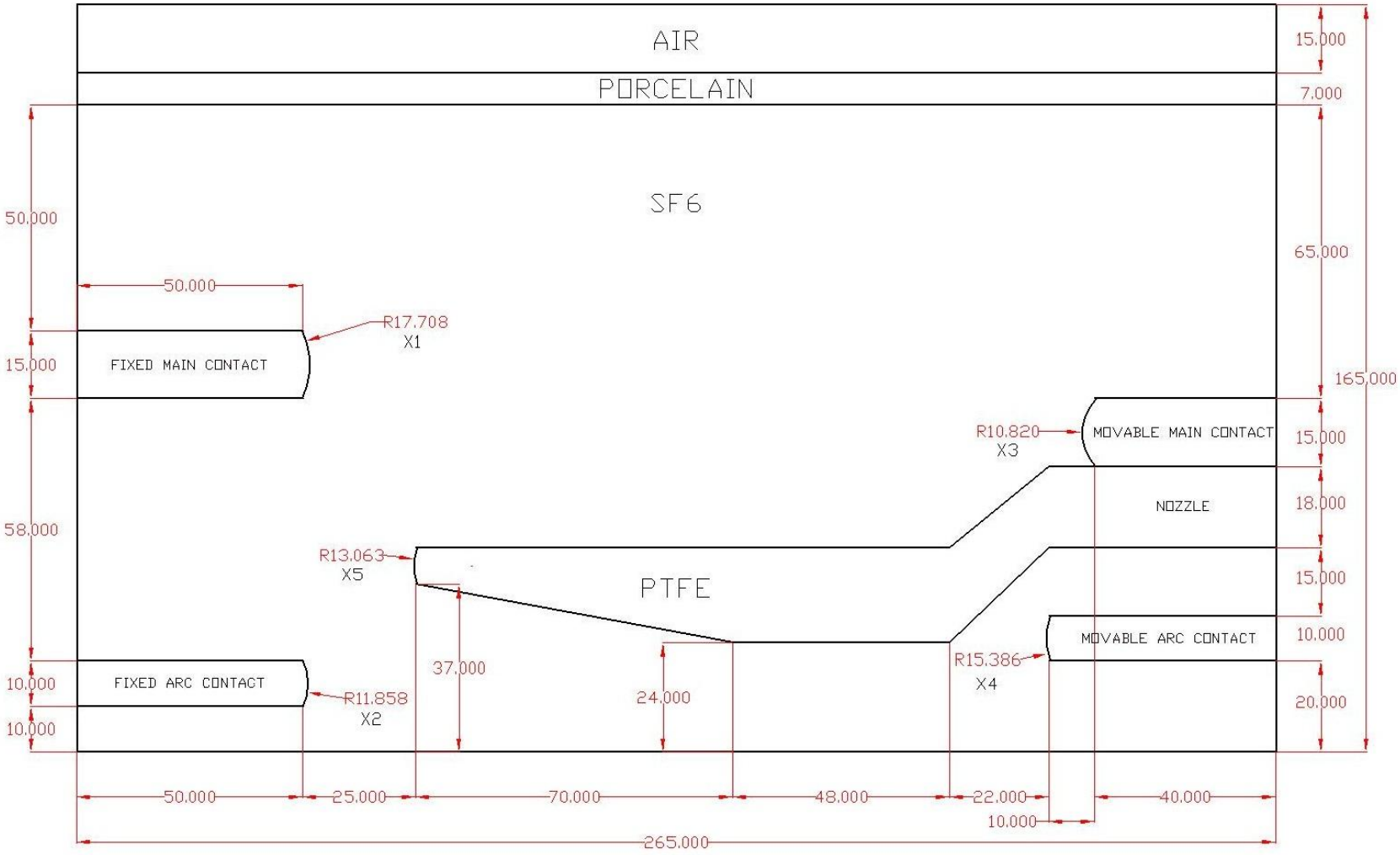

Figure 5.11 ANSYS built-in tool optimized chamber geometry

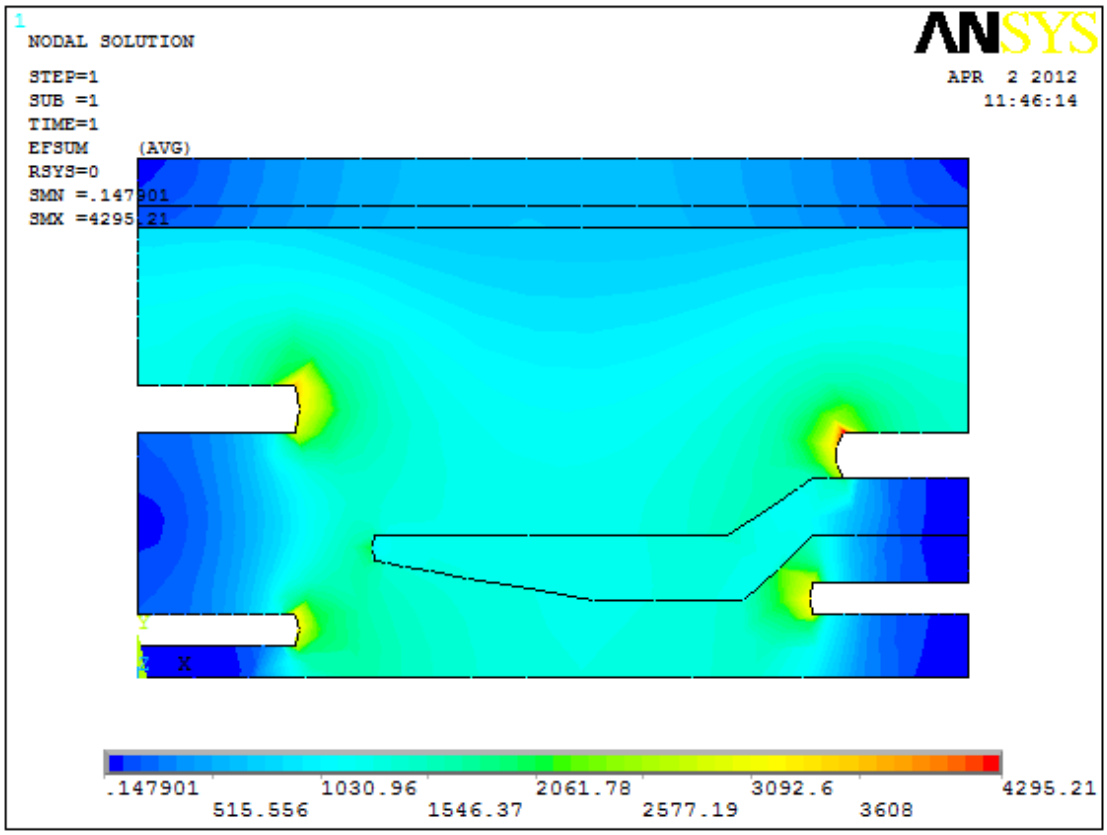

Figure 5.12 Electric field contour for the ANSYS built-in tool optimized geometry

As shown in the above figure, the maximum electric field obtained by solving the ANSYS built-in optimized geometry is (4295.21 V/mm) at the movable main contact. This is a reduction of 7.36% from the non optimized geometry value.

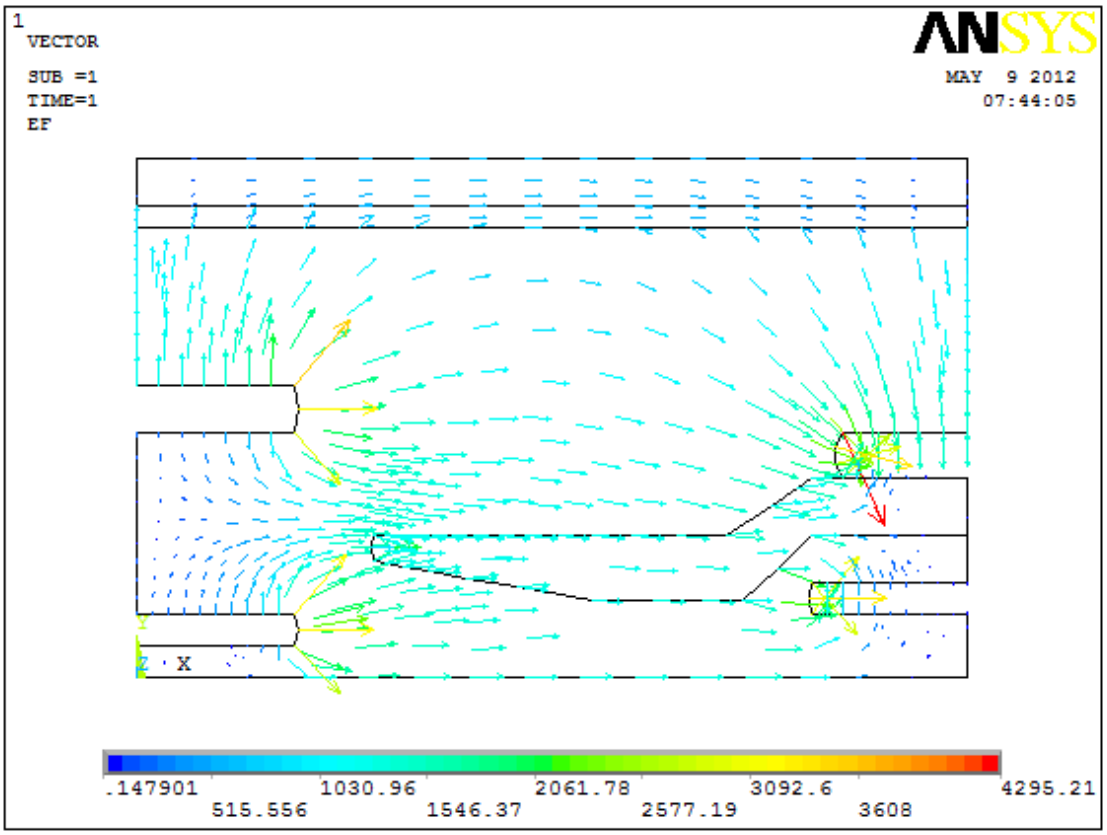

Figure 5.13 Electric field contour for the ANSYS built-in tool optimized geometry

In order to give more insight about the electric field reduction at the most critical points in the circuit breaker, node 1 to 4 are assigned in Fig 5.14 to compare the performance of the proposed optimization algorithms. Comparison between the maximum electric field at the nodes is summarized in Table 5.4. Also Fig 5.15 shows the same comparison.

From the figure and table, it is quite clear that using the proposed optimization algorithms the maximum electric field is generally reduced and is almost uniform at all critical parts of the circuit breaker. On the other hand the ANSYS built-in optimization reduced the electric field at some points and not all of them.

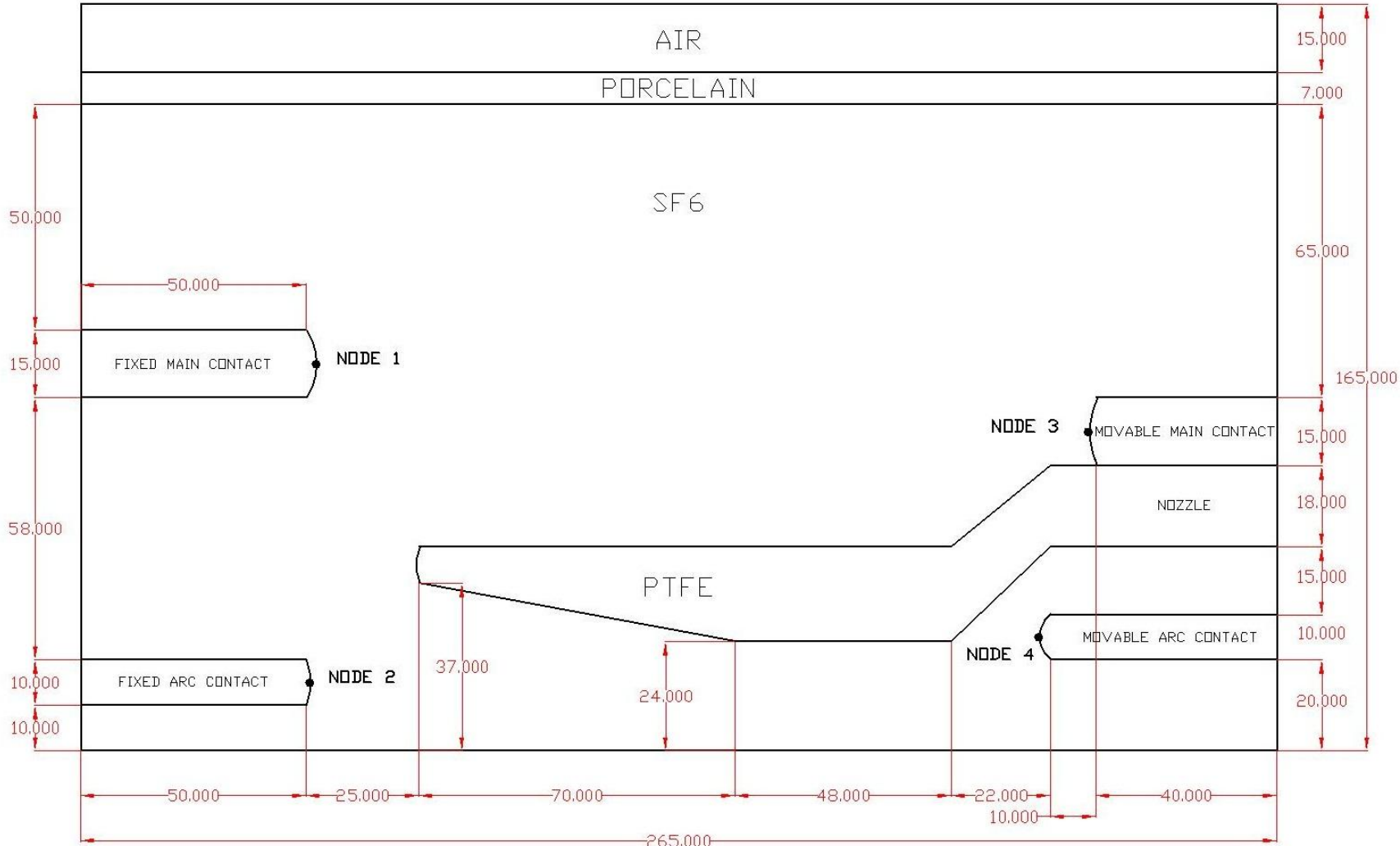

Figure 5.14 the actual location for node 1, 2, 3 and 4

Table 5.4 electric field magnitude in (V/mm) at different nodes for different geometries

The used optimization technique	**Node number**			
	[**1**]	[**2**]	[**3**]	[**4**]
(None) Initial solution	3366.23	2992.78	2922.19	4636.61
(Particle Swarm) solution	3080.54	2826.18	2420.9	2883.19
(Simulated Annealing) solution	3093.14	2864.8	2441.36	2892.8
(Literature [1]) solution	3247.5	3195.6	3378.7	3269.8

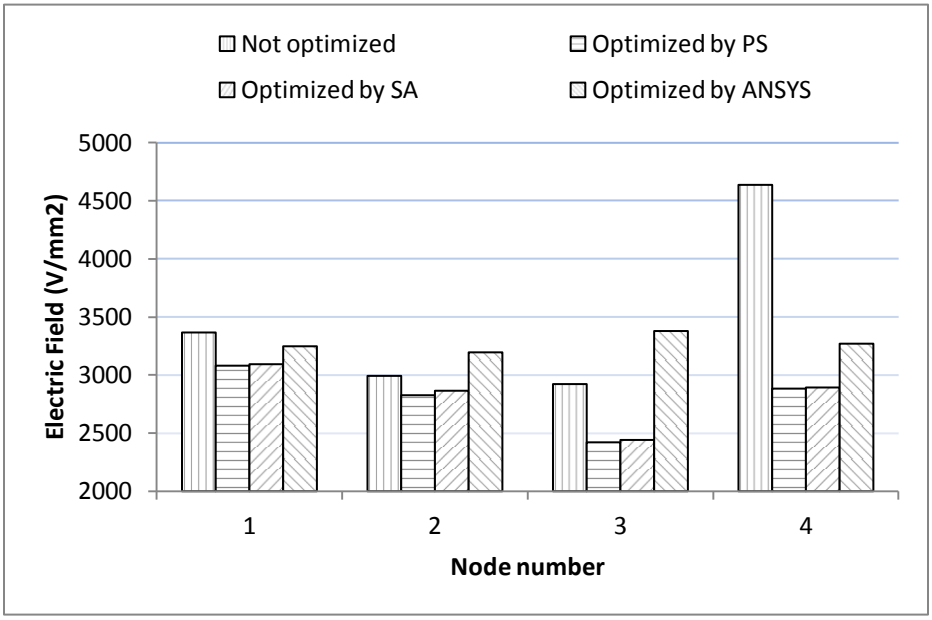

Figure 5.15 electric field magnitude at different nodes for different geometries

5.1.2 Optimizing Electric Field Using Poisson's Equation.

In this case the charge density was included and Poisson's equation was solved in ANSYS by finite element method. The optimum electric fields were obtained by (PS) technique for different values of charge density, Table 5.5 summarizes the results.

Table 5.5 optimized maximum electric field strength for different charge densities using (PS) optimization

Charge density (PC/mm2)	Fixed main contact radius (mm)	Fixed arc contact radius (mm)	Movable main contact radius (mm)	Movable arc contact radius (mm)	Nozzle radius (mm)	Maximum electric field (V/mm)
	$[x_1]$	$[x_2]$	$[x_3]$	$[x_4]$	$[x_5]$	$[J]$
0	23.316	22.57	23.316	22.57	22.272	3292.26
10	24.676	24.082	24.676	24.082	23.844	3386.54
20	24.356	23.726	24.356	23.726	23.474	3587.2
30	25.075	24.525	25.075	24.525	24.305	3791.25
40	25.309	24.785	25.309	24.785	24.576	3985.49
50	24.722	24.133	24.722	24.133	23.898	4184.8
60	25.411	24.899	25.411	24.899	24.694	4384.8
70	25.357	24.839	25.357	24.839	24.632	4584.18

80	24.676	24.082	24.676	24.082	23.844	4783.89
90	24.356	23.726	24.356	23.726	23.474	4985
100	25.357	24.839	25.357	24.839	24.632	5183.15

From the results tabulated in Table 5.5, it is quite clear the presence of space charge increases the maximum electric field in the circuit breaker.

5.2 Case 2 : 550 kV SF6 CB [43]

The second benchmark circuit breaker used to test the performance of the proposed solution algorithms is the one reported by Liu et al [43].

The CB configuration with geometry values are given in Fig. 5.16.

The parameters to be optimized are x_1, x_2, x_3 and x_4. The description of theses parameters and their constrains are given in Table 5.6.

Table 5.6 The optimized parameters constrains'

Constrains range	Movable arc contact radius 1 (mm)	Movable arc contact radius 2 (mm)	Fixed arc contact radius 1 (mm)	Fixed arc contact radius 2 (mm)
	$[x_1]$	$[x_2]$	$[x_3]$	$[x_4]$
Minimum	7.9	7.6	7.3	3
Maximum	30	30	30	30

The effectiveness of the proposed optimization algorithm has been demonstrated by comparing the current optimized results with those reported before [43].

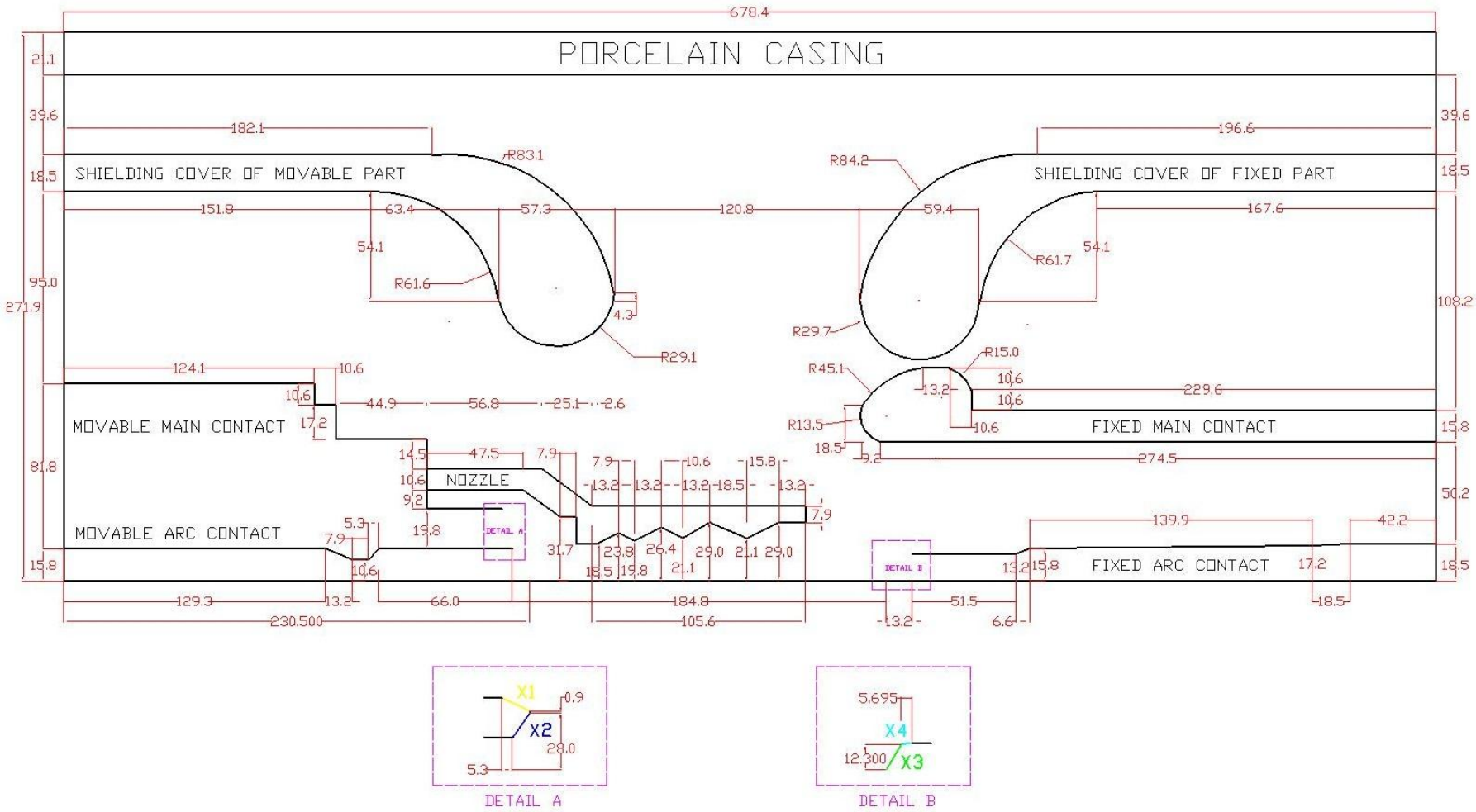

Figure 5.16 Non-optimized chamber geometry

5.2.1 Optimizing Electric Field Using Laplace's Equation.

Using the proposed ANSYS-PS and ANSYS-SA algorithms, the optimized parameters as well the non optimized and previous parameters reported in the literature [43] are shown in Table 5.7. It is worth mentioning that in [43] Variable Interval Genetic Algorithm (VIGA) has been used an optimization tool.

Table 5.7 Maximum electric field strength for different contacts and nozzle radius

The used optimization technique	Movable arc contact radius 1 (mm)	Movable arc contact radius 2 (mm)	Fixed arc contact radius 1 (mm)	Fixed arc contact radius 2 (mm)	Maximum electric field (V/mm) Objective	Maximum electric field reduction (%)
	$[x_1]$	$[x_2]$	$[x_3]$	$[x_4]$	$[J]$	
(None) Initial solution	Not mentioned, high value (straight line)				12337.8	0.0
(Particle Swarm) solution	8.397	8.103	7.81	3.607	7333.24	40.56
(Simulated Annealing) solution	8.471	8.179	7.887	3.698	7296.18	41.05
(Literature [5]) Solution (VIGA)	Not mentioned				7749.37	37.19

It is quite clear that the two proposed algorithms (PS) and (SA) outperform the optimization method reported before [43]. The (PS) electric field reduction reaches (40.56%), while the (SA) electric field reduction reaches (41.05%).

This is a good reduction when compared to the method in the literature (37.19%) reduction. Again this example shows the superior performance of the proposed algorithm.

The schematic diagram for the non-optimized geometry, the electric field contour and vector plotting are shown in Fig. 5.16, Fig 5.17 and Fig 5.18 respectively.

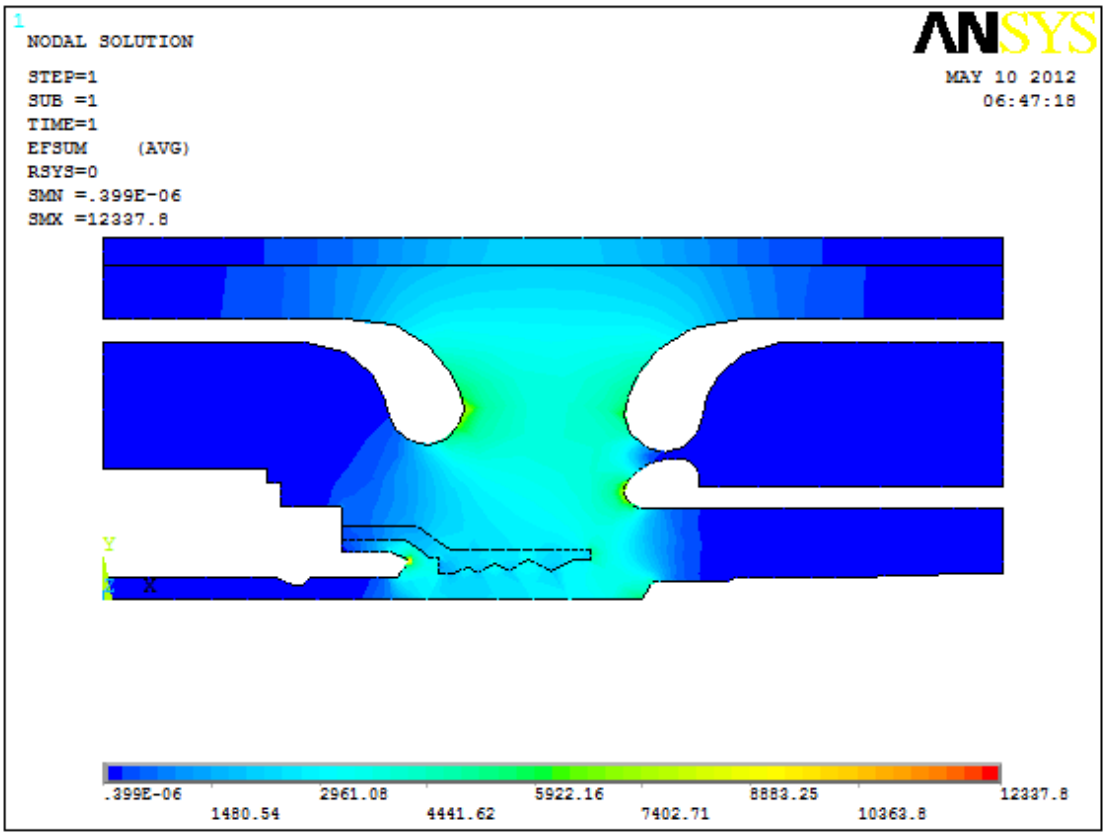

Figure 5.17 Electric field contour for the non-optimized geometry

As shown in the above figure, the maximum electric field obtained by solving the non-optimized geometry is (12337.8 V/mm) at the movable arc contact.

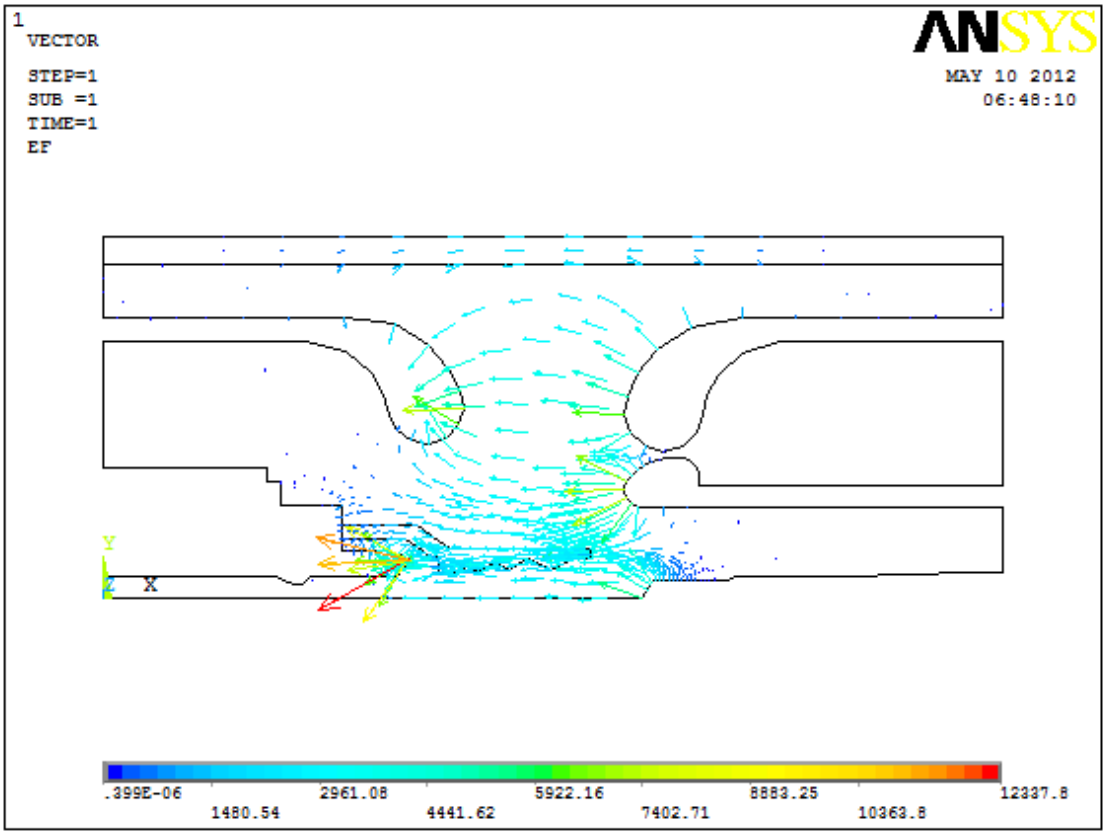

Figure 5.18 Electric field vector for the non-optimized geometry

On the other hand, Fig. 5.19, Fig 5.20 and Fig 5.21 show schematic diagram for the optimized geometry, electric field contour and field plotting for the (PS) optimized geometry respectively.

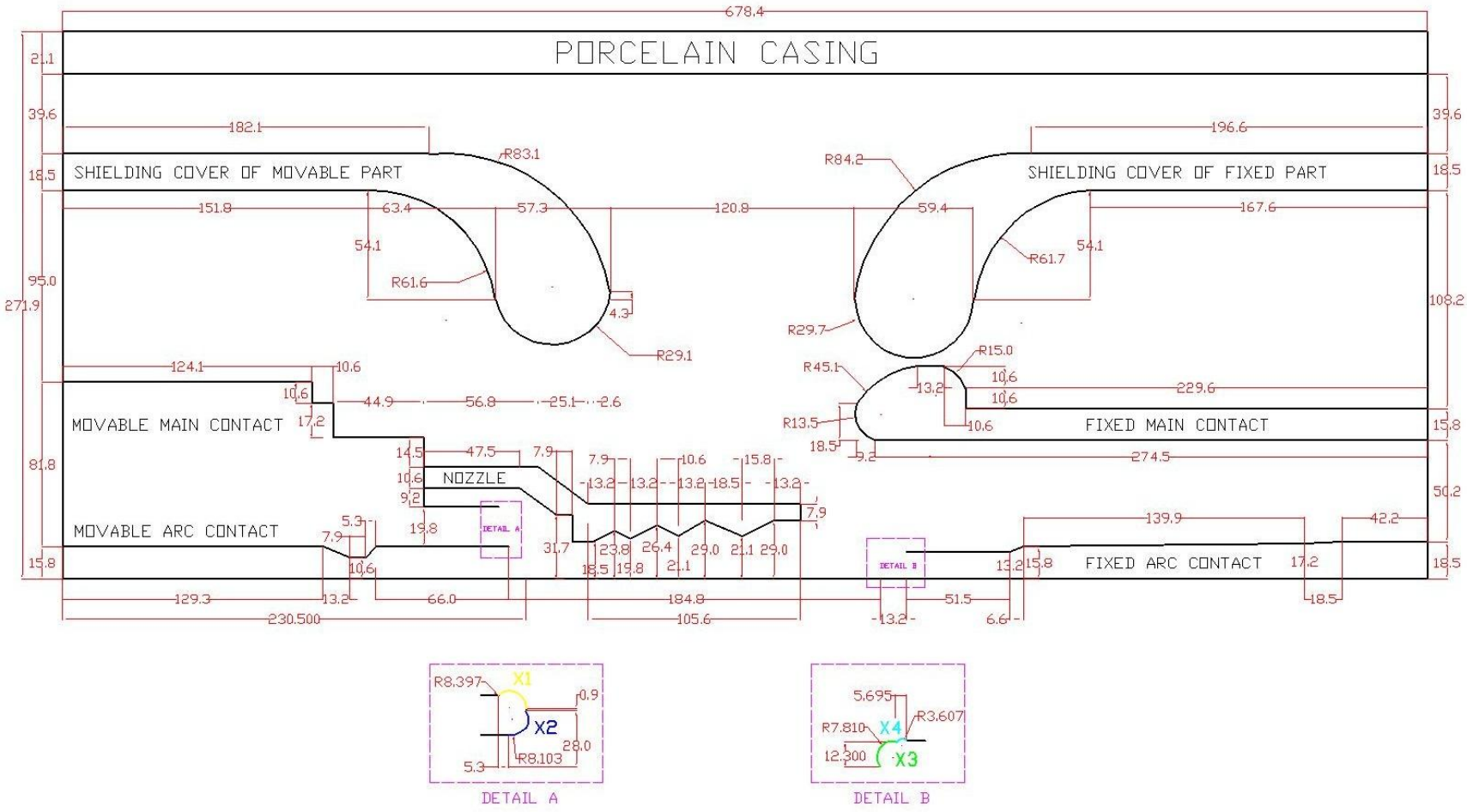

Figure 5.19 PS optimized chamber geometry

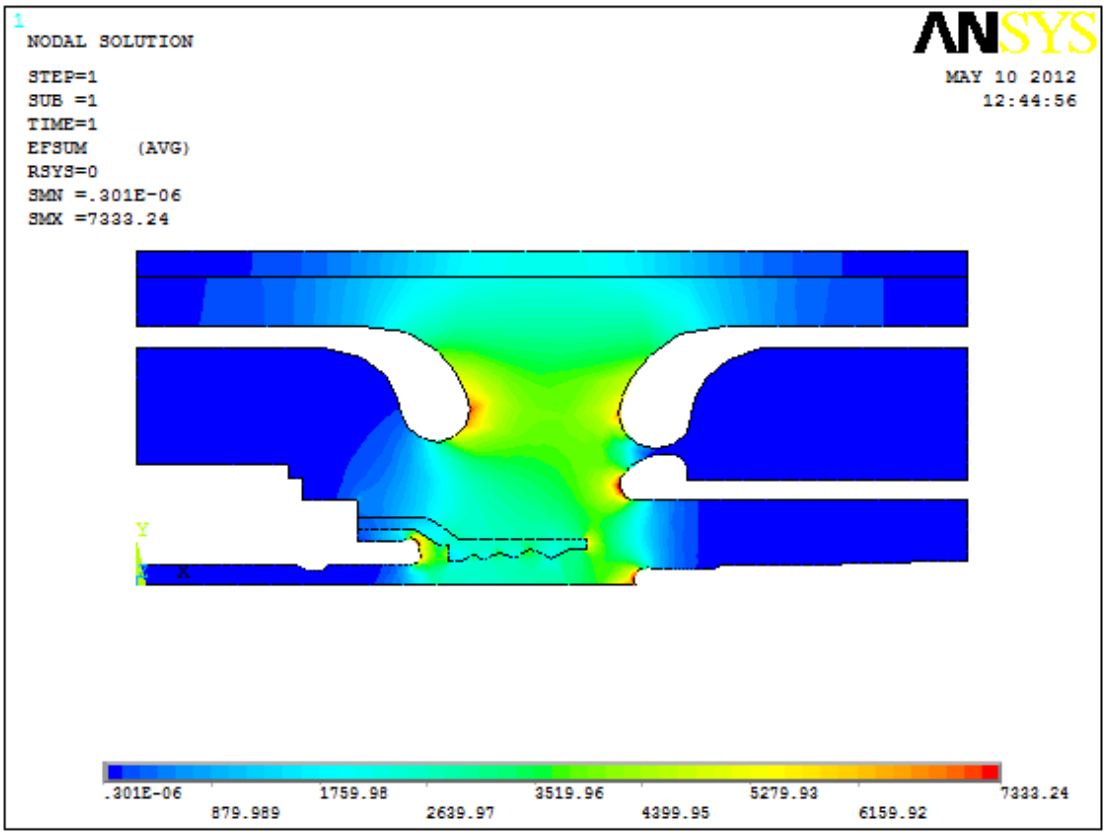

Figure 5.20 Electric field contour for (PS) optimized geometry

It is quite clear from Fig. 5.20 that the maximum electric field obtained by solving the (PS) optimized geometry is (7333.24 V/mm) at the fixed main contact. This is a reduction of 40.56% from the non optimized geometry value.

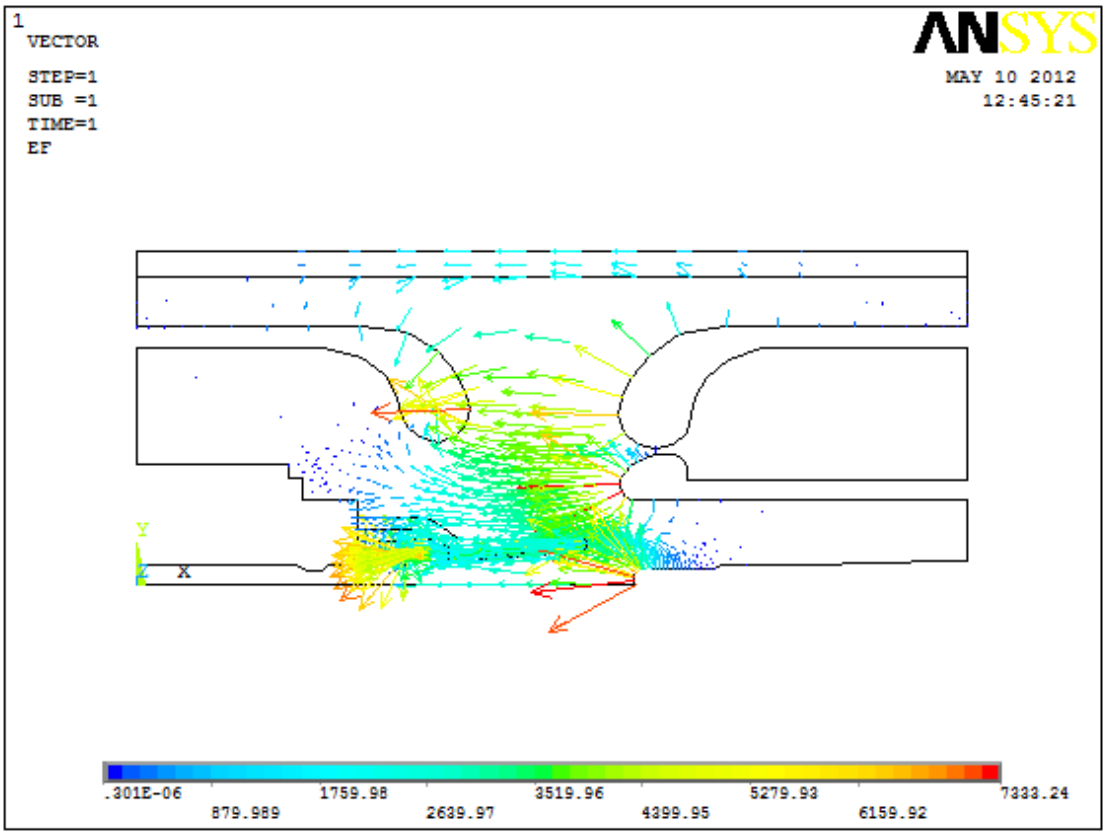

Figure 5.21 Electric field vector for (PS) optimized geometry

The same initial geometry was optimized to minimize the maximum electric field using (SA) algorithm. Fig. 5.22, Fig 5.23 and Fig 5.24 show schematic diagram for the optimized geometry, electric field contour and field plotting for the (SA) optimized geometry respectively.

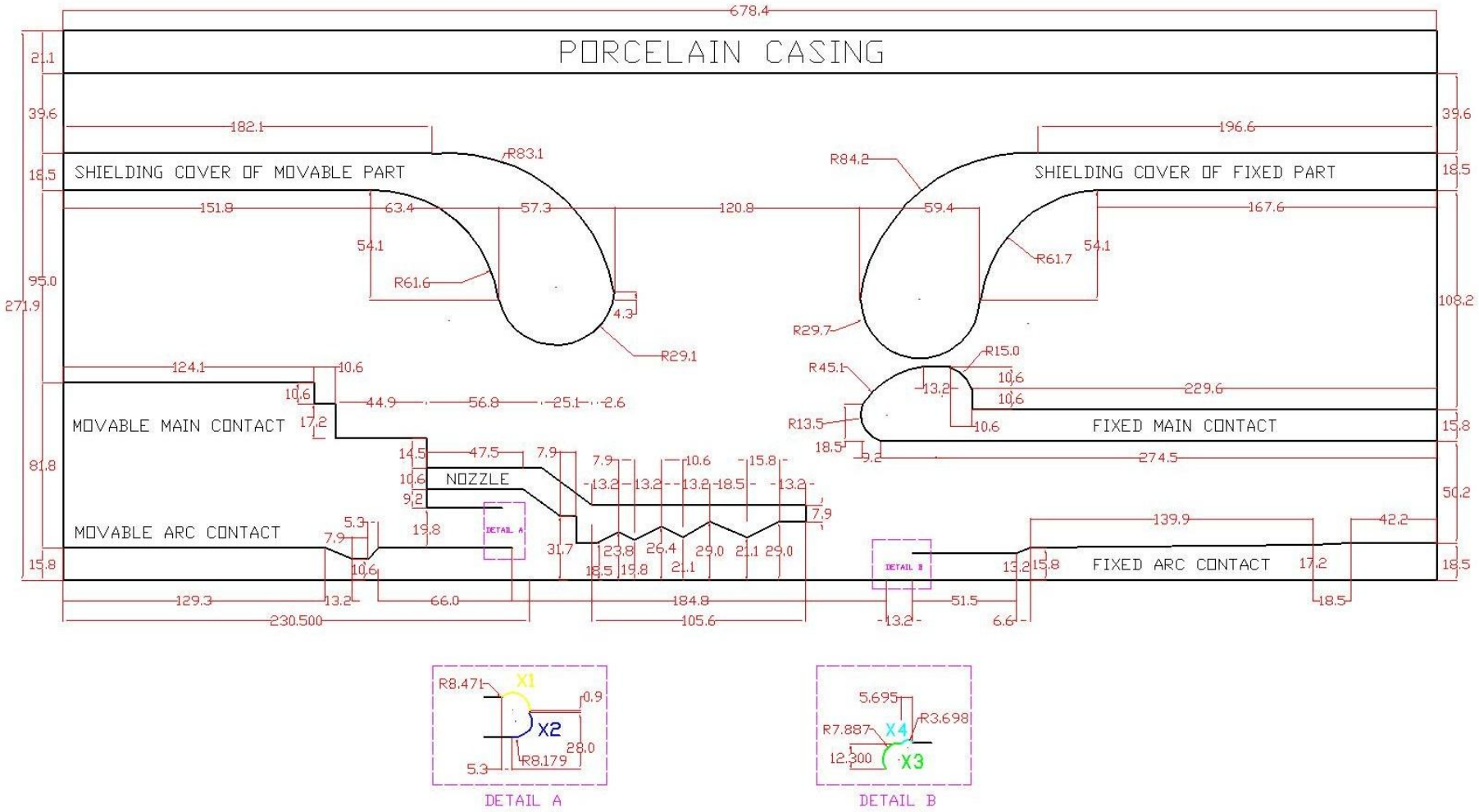

Figure 5.22 SA optimized chamber geometry

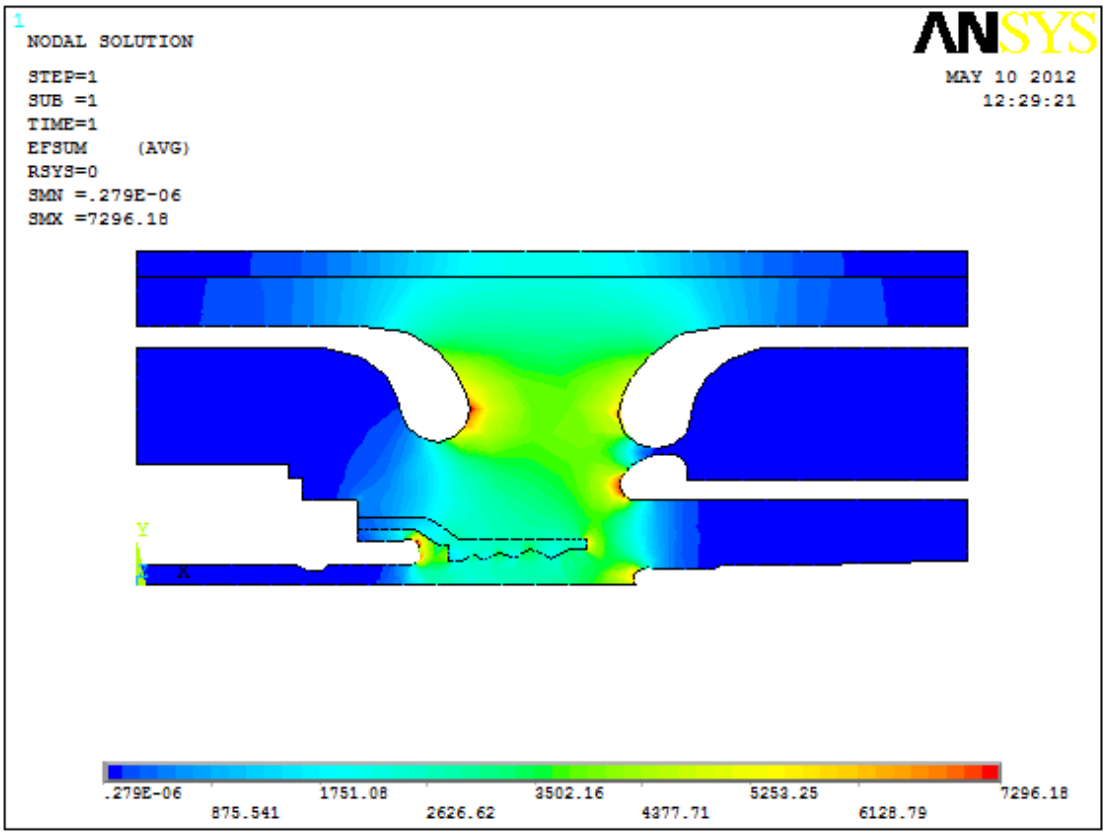

Figure 5.23 Electric field contour for the (SA) optimized geometry

As shown in the above figure, the maximum electric field obtained by solving the (SA) optimized geometry is (7296.18 V/mm) at the movable main contact. This is a reduction of 41.05% from the non optimized geometry value.

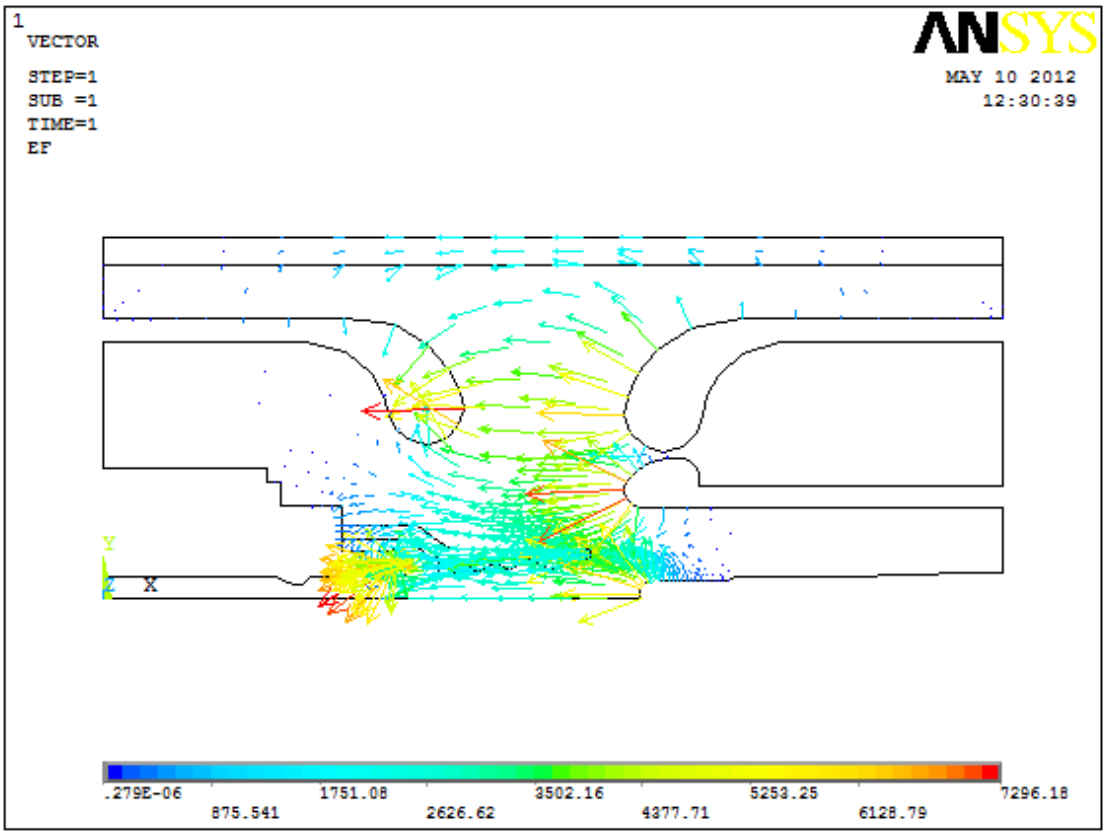

Figure 5.24 Electric field vector for the (SA) optimized geometry

In order to give more insight about the electric field reduction at the most critical parts in the circuit breaker, part 1 to 5 are assigned in Fig 5.25, comparison between the maximum electric field at these parts is summarized in Table 5.8. Also Fig 5.26 shows the same comparison.

It is quite clear that using the proposed optimization algorithms the maximum electric field is reduced at all critical parts of the circuit breaker.

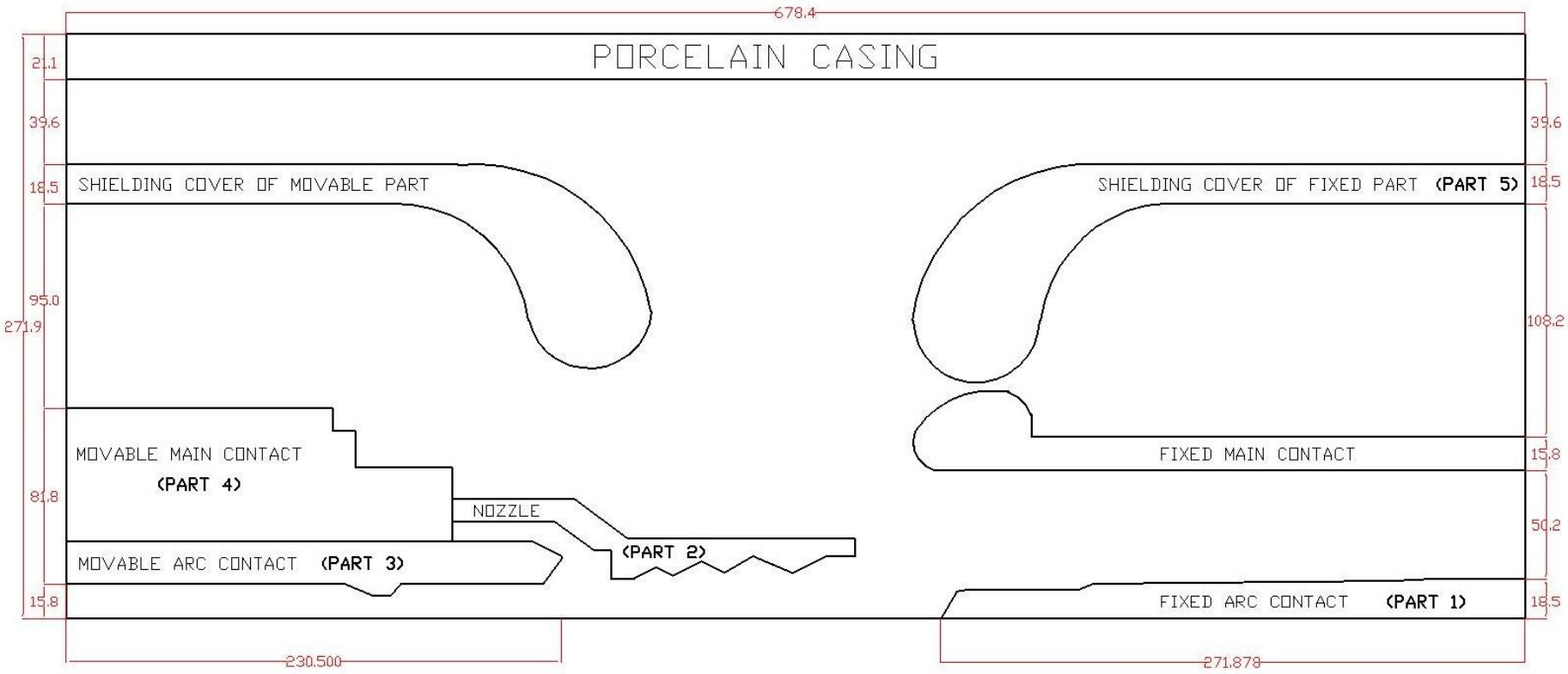

Figure 5.25 the actual location for part 1, 2, 3, 4, and 5

Table 5.8 Maximum electric field magnitude in (V/mm) at different parts for different geometries

The used optimization technique	**Node number**				
	[1]	**[2]**	**[3]**	**[4]**	**[5]**
(None) Initial solution	9500	12394	7000	5500	7000
(Particle Swarm) solution	5439.35	4993.58	6032.17	476.707	6409.66
(Simulated Annealing) solution	5905.63	5648.45	6638.98	474.775	6205.06
(Literature [5]) Solution (VIGA)	8000	6000	7000	500	6500

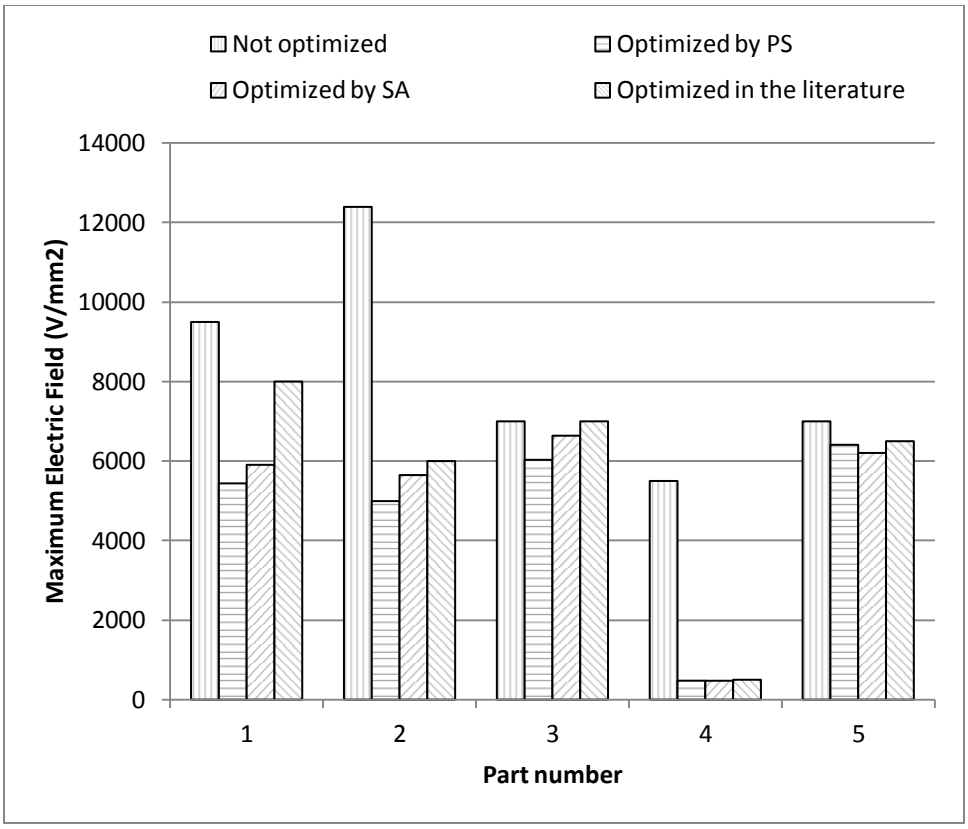

Figure 5.26 Maximum electric field magnitude at different parts for different geometries

5.2.2 Optimizing Electric Field Using Poisson's Equation.

In this case the charge density was included and Poisson's equation was solved in ANSYS by finite element method, the optimum electric fields were obtained by (PS) technique for different values of charge density, Table 5.9 summarizes the results.

Table 5.9 Optimized maximum electric field strength for different charge densities using (PS) optimization

Charge density (PC/mm2)	Movable arc contact radius 1 (mm)	Movable arc contact radius 2 (mm)	Fixed arc contact radius 1 (mm)	Fixed arc contact radius 2 (mm)	Maximum electric field (V/mm)
	$[x_1]$	$[x_2]$	$[x_3]$	$[x_4]$	$[J]$
0	8.397	8.103	7.81	3.607	7333.24
10	8.397	8.103	7.81	3.607	7390.82
20	8.397	8.103	7.81	3.607	7529.54
30	8.397	8.103	7.81	3.607	7668.26
40	8.397	8.103	7.81	3.607	7806.98
50	8.531	8.24	7.948	3.771	8056.26
60	8.397	8.103	7.81	3.607	8084.42
70	8.397	8.103	7.81	3.607	8223.14

80	9.636	9.36	9.083	5.121	8476.23
90	8.531	8.24	7.948	3.771	8641.24
100	8.564	8.273	7.982	3.812	8780.23

It can be noticed from Table 5.9 that most of the optimized solutions are identical.

It is worth mentioning that the previous proposed algorithms converge to the optimal values very quickly as compared to the work reported in [43].

For example, the optimization time for (PS) is about 5 minutes and for (SA) about 1 hour compared to more than 8 hours reported in [43].

This is in spite of the number of nodes used in the current work (3000 nodes) as compared to (130 nodes) in [43]. This increase in the number of nodes improves the accuracy without affecting the computational time.

CHAPTER 6

CONCLUSIONS AND RECOMMENDATIONS

1. Formulation of the electric field in the CB as an optimized problem.
2. For the first time artificial inelegance namely: particle swarm (PS) and simulated annealing (SA) are used along with ANSYS to solve such an optimization problem.
3. The effectiveness of the newly proposed electric field optimization algorithms has been tested successfully on two SF6 CB's (252 kV and 550 kV) reported in the literature [1] and [43] respectively.
4. The performance of the proposed ANSYS-PS and ANSYS-SA methods outperformed the optimization results reported before.
5. Not only the electric field is highly reduced using the proposed algorithms but also the computation time is tremendously reduced too.
6. The effect of space charge on the performance of the proposed algorithms has been tested.
7. It is recommended to include more practical space charge density and investigate the performance of the proposed algorithms.

REFERENCES

[1] H. Miao, H. Wang and Y. Xu "The Numerical Calculation and Optimization Design of Electric Field for the High Voltage SF6 Circuit Breaker Arc-quenching Chamber," Sustanble Power Generation and Supply (SUPERGEN'09), International Conference on 6-7 April 2009.

[2] E. L. Brancato, "Insulation Aging a Historical and Critical Review," IEEE Transactions on Electrical Insulation, Vol. EI-13. No. 4, August 1978.

[3] M. Leijon, M. Dahlgren, L. Walfridsson, L. Ming and A. Jaksts, "A Recent Development in the Electrical Insulation Systems of Generators and Transformers," IEEE Electrical Insulation Magazine,Vol. 17. No. 3, May-June 2001.

[4] I. Fofana, V. Wasserberg, H. Borsi and E. Gockenbach, "Challenge of Mixed Insulating Liquids for Use in High-Voltage Transformers, Part 1: Investigation of Mixed Liquids," IEEE Electrical Insulation Magazine, Vol. 18. No. 3, May/June 2002.

[5] Y. Kawaguchi, H. Murata and M. Ikeda, "Breakdown of Transformer Oil," IEEE Transactions on Power Apparatus and systems, Vol. PAS-91. Issue: 1, Jan. 1972.

[6] B.L. Qin, G.Z. Chen, Q. Qiao and J.N. Sheng, "Effiecient Computation of Electric Field in High Voltage Equipment," IEEE Transactions on Magnetics, Vol. 26. No. 2, March 1990.

[7] A. H. Cookson, O. Farishand and G. M. L. Sommerman, "Effect of Conducting Particles on AC Corona and Breakdown in Compressed SF6," IEEE Transactions on Power Apparatus and systems, Vol. PAS-91. Issue: 4, July 1972.

[8] C. M. Cooke, R. E. Wootton and A. H. Cookson, "Influence of Particles on AC and DC Electrical Performance of Gas Insulated Systems at Extra-High-Voltage," IEEE Transactions on Power Apparatus and System , Vol. PAS-96, No. 3, May/June 1977.

[9] A. H. Cookson, "Particle-Initiated Breakdown Between Coaxial Electrodes in Compressed SF6," IEEE Transactions on Power Apparatus and systems, Vol. PAS-92. Issue: 3, May 1973.

[10] C. M. Cooke and A. H. Cookson, "The Nature and Practice of Gases As Electrical Insulators," IEEE Transactions on Electrical Insulation, Vol. EI-13, No. 4, August 1978.

[11] T. Uchii, T. Nakamoto, T. Nishiwaki, M. Toyoda and S. A Bogg "Optimization of Dead Tank Gas Circuit Breaker Design Based on Quantification of Hot Gas Flow and Dielectric Properties," IEEE Transaction on Power Delivery, Vol. 19, No. 1, January 2004.

[12] G. J. Cliteur, Y. Hayashi, E. Haginomori, and K. Suzuki, "Calculation of the Uniform Breakdown Field Strength of SF6 Gas," IEEE Transaction Dielectric and Electrical Insulation, Vol. 5. pp. 843-849, Dec. 1998.

[13] M. Farahani, H. Borsi and E. Gockenbach, "Dielectric Response Studies on Insulating System of High Voltage Rotating Machines," IEEE Transactions on Dielectrics and Electrical Insulation Vol. 13, No. 1, February 2006.

[14] M. Farahani, H. Borsi, E. Gockenbach and M. Kaufhold, "Partial Discharge and Dissipation Factor Behavior of Model Insulating Systems for High Voltage

Rotating Machines Under Different Stresses," IEEE Electrical Insulation Magazine, Vol. 21. No. 5, September/October 2005.

[15] W. Pfeiffer, "High-frequency Voltage Stress of Insulation," IEEE Transactions on Electrical Insulation, Vol. 26. No. 2, April. 1991.

[16] C. Volat and M. Farzaneh, "Three-Dimensional Modeling of Potential and Electric-Field Distributions Along an EHV Ceramic Post Insulator Covered With Ice Part I: Simulations of a Melting Period," IEEE Transactions on Power Delivery, Vol. 20. No. 3, July 2005.

[17] N. Hozumi, H. Suzuki, T. Okamoto, K. Watanabe and A. Watanabe, "Direct Observation of Time-dependent Space Charge Profiles in XLPE Cable under High Electric Fields," IEEE Transactions on Electrical Insulation, Vol. 1. No. 6, December 1994.

[18] Y. Cao, P. C. Irwin and K. Younsi, "The Future of Nanodielectrics in the Electrical Power Industry," IEEE Transactions on Electrical Insulation, Vol. 11, No. 5, October 2004.

[19] F. Gutfleisch, H. Singer, K. Förger, and J. A. Gomollon, "Calculation of High-Voltage Fields by Means of the Boundary Element Method," IEEE Transaction on Power Delivery, Vol. 9. No. 2, April 1994.

[20] S. Kaana-Nkusi, P. H. Alexander and R. Hackam, "Potential and Electric Field Distributions at a High Voltage Insulator Shed," IEEE Transactions on Electrical Insulation, Vol. 23 No. 2, April 1988.

[21] T. Zhao, and M. G. Comber, "Calculation of Electric Field and Potential Distribution Along Nonceramic Insulators Considering the Effects of Conductors and

Transmission Towers," IEEE Transactions on Power Delivery, Vol. 15, No. 1, January 2000.

[22] H. M. Ryan, J. M. Mattingley and M. F. Scott, "Computation of Electric Field Distributions in High-Voltage Equipment," IEEE Transactions on Electrical Insulation, Vol. EI-6. No. 4, Dec. 1971.

[23] N. H. Malik and A. H. Qureshi, "A Review of Electrical Breakdown in Mixtures of SF6 and Other Gases," IEEE Transactions on Electrical Insulation, Vol. EI-14. No. 1, Feb. 1979.

[24] S. Yanabu, Y. Murayama and S. Matsumoto, "SF6 Insulation and its Application to HV Equipment," IEEE Transactions on Electrical Insulation, Vol. 26. No. 3, June. 1991.

[25] A. A. Azer and R. P. Comsa, "Influence of Field Nonuniformity on the Breakdown Characteristics of Suliur Hexafluoride," IEEE Transactions on Electrical Insulation, Vol. EI-8. No. 4, Dec. 1973.

[26] S. Yanabu, E. Zaima, and T. Hasegawa, "Historical Review of High Voltage Switchgear Developments in the 20th Century for Power Transmission and Distribution System in Japan," IEEE Transactions on Power Delivery, Vol. 21. No. 2, April 2006.

[27] B.F. Hampton and R.J. Meats, "Diagnostic Measurements at UHF in Gas Insulated Substations," IEE Proceedings, Vol. 135, Pt. C , No. 2, MARCH I988.

[28] J. Sato, T. Shioiri, M. Miyagawa, T. Yoshida and K. Yokokura, "Composite Insulation Technology for New Compact 72/84kV C-GIS," IEEE Transmission and Distribution Conference, Vol. 2, 11-16 Apr 1999.

[29] R. Vogelsang, T. Weiers, K. Fröhlich and R. Brütsch, "Electrical Breakdown in High-Voltage Winding Insulations of Different Manufacturing Qualities," IEEE Electrical Insulation Magazine, Vol. 22. No. 3, May/June 2006.

[30] Z. Andjelic and S. Sadovic, "Reduction of Breakdown Appearance by Automatic Geometry Optimization," Conference on Electrical Insulation and Dielectric Phenomena, CEIDP. 2007, 14-17 Oct. 2007.

[31] F. Messerer and W. Boeck, "High Resistance Surface Coating of Solid Insulating Components for HVDC Metal Eeclosed Equipment," Eleventh International Symposium on High Voltage Engineering, Vol. 4, 22-27 August 1999.

[32] R. Parashar, A. Baker and A. Sitzia, "Challenges For Vacuum Interrupter Design," ISDEIV. XXIInd International Symposium on Discharges and Electrical Insulation in Vacuum, Vol. 2, 25-29 Sept. 2006.

[33] M. Yousfi, Ph. Robin-Jouan and Z. Kanzari, "Breakdown Electric Field Calculations of Hot SF6 for High Voltage Circuit Breaker Applications," IEEE Transactions on Dielectrics and Electrical Insulation, Vol. 12, No. 6, December 2005.

[34] F. Endo, M. Sato, M. Tsukushi, Y. Yoshioka, K. Saito and K. Hirasawa, "Analytical Prediction of Transient Breakdown Characteristics of SF6 Gas Circuit Breakers," IEEE Transactions on Power Delivery, Vol. 4, No. 3, July 1989.

[35] T. Nitta and Y. Shibuya, "Eelectrical Breakdown of Long Gaps in Sulfur Hexafluoride," IEEE Transactions on Power Apparatus and systems, Vol. PAS-90. Issue: 3, May 1971.

[36] H. Okubo, "Development of Electrical Insulation Techniques in Vacuum for Higher Voltage Vacuum Interrupters," ISDEIV. XXIInd International Symposium on Discharges and Electrical Insulation in Vacuum, Vol. 1, 25-29 Sept. 2006.

[37] T. Shioiri, M. Honma, E. Kaneko, M. Miyagawa and I. Ohshima, "Insulation Characteristics of Vacuum Interrupter for a New 72/84 kV C-GIS," ISDEIV. XVIIIth International Symposium on Discharges and Electrical Insulation in Vacuum, Vol. 2, 17-21 Aug 1998.

[38] U. Schumann, S. Giere and M. Kurrat, "Breakdown Voltage of Electrode Arrangements in Vacuum Circuit Breakers," IEEE Transactions on Dielectrics and Electrical Insulation, Vol. 10, No. 4, August 2003.

[39] Y. Murai, H. Toya and T. Nitta, "Statistical Property of The Breakdown of Vacuum Circuit Breakers and Its Influence on The Surge Generation in Capacitive and Reactive Current Interruption," IEEE Transactions on Power Apparatus and Systems, Vol. PAS-98, No.1 Jan/Feb 1979.

[40] S. Monga, R. S. Gorur, P. Hansen and W. Massey, "Design Optimization of High Voltage Bushing Using Electric Field Computations," IEEE Transactions on Dielectrics and Electrical Insulation, Vol. 13, No. 6, December 2006.

[41] C. Trinitis, "Field Optimization of Three Dimensional High Voltage Equipment," Eleventh International Symposium on High Voltage Engineering, Vol. 2, 22-27 August 1999.

[42] M. Abd-Elsalam and M. M. Abouelsaad, "A New Method for Optimization of High Voltage Electrode Surfaces using Genetic Algorithms," Alexandria Engineering Journal, Vol. 42 (2003), No. 2, 201-208.

[43] X. Liu, Y. Cao, F. Wen, and E. Wang, "Optimization of Extra High Voltage SF6 Circuit Breaker Based on Improved Genetic Algorithm," IEEE Transaction on magnetics, Vol. 44,No. 6, June 2008.

[44] Z. Zhizhong, Z. Jiyan, W. Huabin and Sun Hui "Utility Optimization Method of a High Voltage Vacuum Interrupter Design," IEEE Transaction on Dielectric and Electrical Insulation, Vol. 14, No. 3, June 2007.

[45] H. Kojima1, K. Suzuki, K.i Kato and H. Okubo. "Electric Field Optimization of Floating Electrode Configuration in Vacuum Interrupters," High Voltage Engineering and Applications (ICHVE), International Conference on 11-14 October 2010.

[46] Y. Cao, Y. Liu, J. Li, X. Liuand C. Hou "Nozzle Optimization of SF6 Circuit Breaker Based on Artificial Neural Network and Genetic Algorithm," Electrical Machines and Systems (ICEMS), International Conference on 17-20 October 2008.

[47] H. K. Kim, K. Y. Park, C. H. Im, and H. K. Jung, "Optimal Design of Gas Circuit Breaker for Increasing the Small Current Interruption Capacity," IEEE Transaction on magnetics, Vol. 39,No. 3, May 2003.

[48] A. Iturregi, E. Torres, I. Zamora, and O. Abarrategui, "High Voltage Circuit Breakers: SF6 vs. Vacuum," International Conference on Renewable Energies and Power Quality (ICREPQ'09), Valancia (spain), April, 2009.

[49] F. Pinnekamp, "The Circuit Breaker," ABB R&D Group and Technology Zurich, Switzerland, ABB Review 1/2007.

[50] S. S. Rao, “Switchgear protection and power systems,” Khanna Publishers, thirteenth edition, October 2008.

[51] Y. Liu, “Introduction to The Finite Element Method,” CAE Research Laboratory, Mechanichal Engineering Department, University of Cincinnati, Cincinnati USA.

[52] O. D. Weck and I. Y. Kim, “Engineering Design and Rapid Prototyping (Finite Element Method),” Massachusetts Institue of Technology, January 2004.

[53] D. G. Duffy, “Advanced Engineering Mathematics With MATLAB,” Third Edition, CRC Press.

[54] J. Kennedy, "The Particle Swarm: Social Adaptation of Knowledge," Proceedings of the 1997 IEEE international Conference on Evolutionary Computation ICEC'97, Indianapolis, Indiana, USA,1997, pp. 303-308.

[55] P. Angeline, "Evolutionary Optimization versus Particle Swarm Optimization: Philosophy and Performance Differences, " Proc. of the 7th Annual Conf. on Evolutionary Programming, 1998, pp. 601-610.

[56] Y. Shi and R. Eberhart, "Parameter Selection in Particle Swarm Optimization," Proceedings of the 7th Annual Conference on Evolutionary Programming, March 1998, pp. 591-600.

[57] E. Ozcan and C. Mohan, "Analysis of a Simple Particle Swarm Optimization System," Intelligent Engineering Systems Through Artificial Neural Networks, Vol. 8, 1998, pp. 253-258.

[58] N. Metropolis, A. Rosenbluth, M. Rosenbluth, A.Teller, and E. Teller, "Equation of State Calculations by Fast Computing Machines," Journal of Chemical Physics, Vol. 21, 1953, pp. 1087-1092.

[59] E. Aarts and J. Korst, Simulated Annealing and Boltzmann Machines: A Stochastic Approach to Combinatorial Optimization and Neural Computing, John Wiley & Sons, 1989.

VITA

Name: SALEH ABU HANIEH

Place of Birth: Zarqa, Jordan.

Nationality: Jordanian

Permanent Address: Khobar,

Saudi Arabia.

Telephone: +966544834400

Email Address: sale7_yu@yahoo.com

Educational Qualification:

M.S (Electrical Engineering)

June 2012

King Fahd University of Petroleum and Minerals

Dhahran, Saudi Arabia.

B.S (Electrical Power Engineering)

March 2008

Yarmouk University,

Irbid, Jordan.